Applied Physics Reviews REVIEW pubs.aip.org/aip/are

Silicon carbide: A promising platform for scalable quantum networks

Cite as: Appl. Phys. Rev. **12**, 031301 (2025); doi: 10.1063/5.0262377
Submitted: 1 February 2025 · Accepted: 12 June 2025 ·
Published Online: 1 July 2025

Yu Zhou,[1,2,a)] Junhua Tan,[1] HaiBo Hu,[1,3] Sikai Hua,[1] Chunhui Jiang,[1] Bo Liang,[1] Tongyuan Bao,[1] Xinfang Nie,[4] Shumin Xiao,[1,2,3,5] Dawei Lu,[4,a)] Junfeng Wang,[6,a)] and Qinghai Song[1,2,3,5,a)]

AFFILIATIONS

[1]Ministry of Industry and Information Technology Key Lab of Micro-Nano Optoelectronic Information System, Guangdong Provincial Key Laboratory of Semiconductor Optoelectronic Materials and Intelligent Photonic Systems, Harbin Institute of Technology, Shenzhen 518055, People's Republic of China
[2]Quantum Science Center of Guangdong-HongKong-Macao Greater Bay Area (Guangdong), Shenzhen 518045, People's Republic of China
[3]Pengcheng Laboratory, Shenzhen 518055, People's Republic of China
[4]Department of Physics, State Key Laboratory of Quantum Functional Materials, and Guangdong Basic Research Center of Excellence for Quantum Science, Southern University of Science and Technology, Shenzhen 518055, China
[5]Collaborative Innovation Center of Extreme Optics, Shanxi University, Taiyuan 030006, Shanxi, People's Republic of China
[6]College of Physics, Sichuan University, Chengdu 610065, People's Republic of China

Note: This paper is part of the Special Topic, Quantum Light.

[a)]**Authors to whom correspondence should be addressed:** zhouyu2022@hit.edu.cn; ludw@sustech.edu.cn; jfwang@scu.edu.cn; and qinghai.song@hit.edu.cn

ABSTRACT

Quantum networks based on solid-state spin defects present a transformative approach to secure communication and distributed quantum computing, utilizing quantum entanglement and coherent spin–photon interfaces. Silicon carbide (SiC) stands out as a compelling material platform due to its unique combination of a wide bandgap, high optical nonlinearity, CMOS-compatible fabrication, and controllable spin-active defects. These intrinsic properties facilitate efficient photon emission, robust spin coherence at both room and cryogenic temperatures, and integration with photonic nanostructures. Recent advancements in defect engineering and micro-nanophotonics have unlocked the potential of SiC quantum nodes, which feature electron-nuclear spin systems for high-fidelity quantum operations and long-lived quantum memories. Key steps such as single-shot readout and spin-photon entanglement have been successfully demonstrated, bringing SiC closer to a real quantum network platform. This review offers a comprehensive overview of the advancements in SiC-based quantum networks, encompassing key aspects such as defect fabrication methodologies, optimization of spin-photon interfaces, and strategies for photonic integration. Additionally, it examines the existing challenges and outlines promising future directions in this rapidly evolving field.

TABLE OF CONTENTS

I. INTRODUCTION

The development of quantum networks is one of the most exciting frontiers in modern quantum communication technology.[1–4] Unlike classical networks that depend on traditional bits, quantum networks leverage the unique properties of quantum mechanics, such as superposition and entanglement, to create a new paradigm of secure and high-performance communication.[3] In these networks, quantum bits, or qubits, can exist in multiple states at the same time, providing a unique advantage in speed, security, and efficiency. The potential applications of quantum networks reach far beyond secure communications, including groundbreaking advancements in distributed quantum computing, global quantum sensing, and the fabric of the future internet.[5]

As quantum networks rapidly advance, one of the critical challenges is developing reliable and scalable sources of quantum node memories.[6] Since photons are the ideal carriers of quantum information, these nodes must possess highly efficient spin-photon interfaces[7–9] to facilitate the creation of effective quantum networks. Various systems have been explored in building such networks, including superconducting qubits,[10–12] atoms,[13,14] or ions.[4,15,16] Among these candidate systems, quantum defects in silicon carbide (SiC)[17,18] are notable for their capability to easily integrate with existing CMOS-compatible semiconductor technologies, facilitating compact and scalable solutions.[19–22] These defects exhibit long spin coherence times[23] and can be interfaced with photons efficiently.[24,25] Their robustness, adaptability, and compatibility with current infrastructure position them as a strong candidate platform. Additionally, developing SiC photonics[26–29] will facilitate the fabrication and integration of various quantum photonic devices,[30] contributing to the advancement of integrated quantum networks.

Figure 1 shows a schematic diagram of a long-distance quantum network that uses photons as flying qubits within a solid-state color center platform. Quantum nodes (blue spheres) connect through classical channels (solid lines) and quantum channels (dashed lines). The quantum channels establish entanglement between adjacent nodes via heralded photon measurement[31] with subsequent entanglement

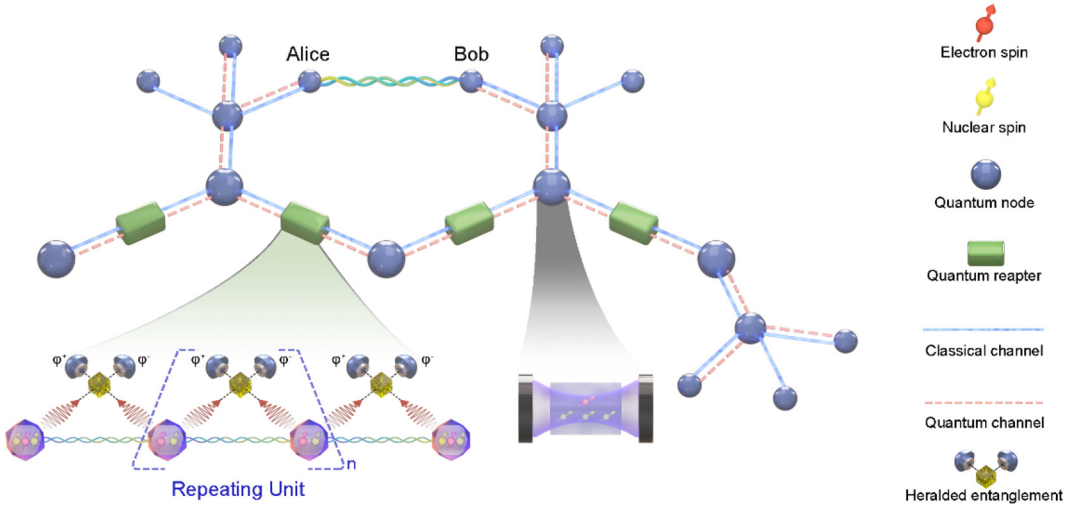

FIG. 1. Schematic illustration of a long-distance quantum network enabled by solid-state quantum defects. The network consists of quantum nodes (blue spheres) connected via classical channels (solid lines) and quantum channels (dashed lines). Entanglement between adjacent nodes is established through heralded photon measurements, while entanglement swapping allows for long-distance connections between Alice and Bob via intermediate nodes. Quantum repeaters (green blocks) facilitate robust entanglement distribution through a hierarchical protocol that includes heralded entanglement generation, swapping, and error mitigation techniques. Each node has electron spins (communication qubits) coupled to nuclear spins (quantum memories), enabling high-fidelity state manipulation, storage, and readout. Spin-photon interfaces, enhanced by optical cavities, improve photon emission efficiency and entanglement generation rates. The architecture emphasizes critical elements for scalable quantum networks, including integrated photonic technologies, efficient spin-photon coupling, and robust quantum memory integration.

swapping[32] enabling long-distance entanglement distribution for end-to-end connection.[33] As the figure demonstrates, the entanglement between Alice and Bob is mediated through intermediate nodes. Through local Bell-state measurements, these remote parties can implement quantum teleportation[34,35] for quantum communication, where classical channels transmit Bell-state measurement outcomes. However, photon transmission over extended distances inevitably suffers from channel loss,[36] leading to exponentially increasing entanglement establishment time with transmission distance.[37] The quantum repeater concept (green blocks in Fig. 1) has been developed[38] to address this limitation. Composed of multiple intermediate nodes (each represented as an electron-nuclear spin system), quantum repeaters enable robust entanglement creation through a hierarchical protocol: initial heralded entanglement generation between adjacent repeater nodes, followed by entanglement swapping[32] for long-distance connection. This architecture incorporates ancillary techniques such as entanglement purification[39–41] and quantum error correction[42–45] to mitigate transmission loss and operational errors.

The proposed quantum network architecture offers a promising solution for multi-node connectivity, although its spatiotemporal scale imposes strict requirements on node capabilities. As shown in Fig. 1, each quantum node (blue sphere) comprises an electron spin (communication qubit) coupled with multiple nuclear spins (ancillary qubits). This configuration allows for high-fidelity spin state manipulation and readout via energy level engineering.[46–48] Nuclear spins serve as quantum memories because of their long coherence times,[49] while demonstrated quantum error correction protocols[42] enhance fault tolerance. These characteristics allow for independent manipulation, processing, and measurement of quantum states at individual nodes without the need for external synchronization. The combination of high-fidelity operations and long coherence times also guarantees reliable local quantum gate operations, a vital prerequisite for future entanglement distribution protocols.[50,51] The spin–photon interface represents a critical element that requires careful engineering of color-center energy structures. Key characteristics include spin-selective optical transitions and microwave addressability,[52] enabling quantum state mapping from spins to photonic degrees of freedom through polarization,[53] frequency,[54] or time-bin encoding.[55] Micro-nanophotonic technologies have been implemented to overcome the inherent low coupling efficiency limitations. As depicted in Fig. 1, integrating spins into high Q factor microcavities greatly enhance light matter interaction.[56–58] The cavity-enhanced architecture enables multiple spin-photon interactions via resonant standing waves modes,[59,60] thereby enhancing photon emission efficiency and entanglement generation rates. For effective long-distance communication, quantum nodes must operate as high-performance single-photon sources. The optical characteristics of these nodes are significantly affected by their local charge environment. Crystal lattice defects and inadequate charge state control can lead to spectral diffusion[61] and reduced photon indistinguishability, adversely affecting Hong-Ou-Mandel interference visibility[62] and entanglement fidelity.[31] Advanced fabrication techniques that maintain crystalline integrity[63–65] combined with active charge state stabilization through p-i-n junction electrical control[66] have proven effective for narrowing spectral linewidth and prolonged spin coherence time.

This review paper is organized as follows: Sec. I introduces the key components involved in constructing defect-based quantum networks. Section II explores various methods for fabricating SiC defects, comparing the optical and quantum properties of color centers across different fabrication techniques. Section III focuses on the spin and photon properties of SiC defects, with particular attention to reducing linewidth and tuning the wavelength for photons, along with the latest techniques for coherent control and readout of electron and nuclear spins for spins. Section IV covers the spin–photon interface in SiC. Section V highlights recent advances in SiC photonics and their advantages in building quantum networks. Finally, Sec. VI reviews the development of quantum networks with defects in diamond and discusses how diamond-inspired architectures can guide the development of SiC's quantum network. Section VII concludes with a discussion of prospects and open challenges.

II. FABRICATION TECHNIQUES OF SPIN DEFECTS IN SiC

There are over 250 polycrystalline types of silicon carbide, with the 3C, 4H, and 6H crystal types being the most common used.[17,18,24,67] Various defects in SiC have been studied and have been shown to exhibit optically addressable transitions, such as silicon vacancy (V_{Si}) center,[68,69] divacancy (VV^0) center,[24,67] vanadium defects (V^{4+}),[70–73] NV center (N_CV_{Si}),[74] carbon antisite–vacancy pair[75] in 4H-SiC, Ky5 in 3C-SiC,[24,76] and undefined single photon sources.[77] These defects have stable and excellent spin and photon properties, making them ideal candidates for qubits. Consequently, effectively fabricating these spin defects without compromising their properties has become critical. The four primary techniques include electron or proton irradiation,[78,79] ion implantation,[80,81] focused particle beam,[82,83] laser writing,[63,84] etc. These fabrication techniques are delineated as follows.

A. Electron or neutron irradiation

High-energy electron or neutron irradiation involves a beam of electrons or neutrons interacting with atoms in a crystal. This process provides sufficient energy to displace certain atoms from their lattice positions, resulting in the formation of lattice defects. The density of color center generation varies depending on the selected irradiation flux. In 2015, Fuchs *et al.* used neutron irradiation (0.18–2.5 MeV) to generate a single V_{si} center with irradiation fluxes ranging from 1×10^9 to $5 \times 10^{17}\,cm^{-2}$.[68] The advantage of electron irradiation is that it does not introduce additional impurities, causes less damage to the lattice, thus enabling longer spin coherence times.[17,25] In 2015, Christle *et al.* irradiated a sample with 2 MeV electrons at varying fluxes (5×10^{12} to $1 \times 10^{15}\,cm^{-2}$) to create VV^0 centers, followed by high-vacuum annealing to reduce lattice damage, exhibiting a Hahn-echo spin coherence time of over 1 ms.[67]

B. Ion implantation

Ion implantation is a widely used technique for introducing defects by injecting ions (such as carbon, hydrogen, and helium). Unlike irradiation, SiC defects are typically produced in a pre-designed array of holes, which allows for intentional control of the color center positions. Specifically, a polymethyl methacrylate (PMMA) mask layer, several hundred nanometers thick, is uniformly spun onto the cleaned surface. Then, a series of hole arrays is created using electron beam lithography (EBL), followed by ion implantation implantation.[85] The accelerated ions cannot penetrate the PMMA-covered area, and color centers are formed in the exposed holes. Depending on the desired defects (single or ensemble), ions are implanted in doses ranging from

10^{11} to 10^{14} cm^{-2}. In 2017, Wang *et al.* created a single V_{Si} defect with an efficiency of about 34% using 30 keV carbon ion implantation through an array with a diameter of 65 nm. The conversion rate of injected carbon ions to V_{Si} was about 19%.[85] The sample was not annealed to avoid producing other defects. Unlike the production of nitrogen-vacancy (NV) centers in diamond, the absence of the annealing step simplifies the process. In 2020, Wolfowicz *et al.* generated a single vanadium center through ^{51}V implantation at 190 keV with stable and narrow emission in the O band.[86] In 2024, Babin *et al.* fabricated silicon vacancies using helium ion implantation. The implantation yield was 8.5%, and the precision was approximately 53 nm in the horizontal plane, which was primarily influenced by the size of the mask hole. Importantly, this work allows for integrating ion-implanted silicon vacancies into waveguides without compromising their inherent spin-optical properties.[87] The primary challenges in scaling spin defect fabrication in SiC—low spatial resolution, poor uniformity—are addressed by emerging techniques like self-aligned nanoscale patterning. Inspired by recent advances in diamond (e.g., ~15 nm precision NV center arrays in diamond), this approach leverages pre-engineered nanostructures (e.g., nanopillars) combined with ion implantation to achieve deterministic defect placement in diamond.[88] Such methods are also applicable to SiC-based spin defects, particularly useful for precise photonic integration.

C. Focused ion beam

In contrast to ion implantation, focused ion beam is a mask-free technique that creates SiC defects by bombarding tiny areas on the nanoscale. It accurately targets the sample surface to create vacancies through ion collisions or to inject impurities into specific locations, making it suitable for nanoscale processing and fixed-point color centers generation.[82,83,89,90] It has the advantage of enabling scalable and deterministic integration of quantum devices.[87] The localization accuracy of defects is determined by the diameter of the focused ion beam (5–10 nm) and the transverse discretization effect of silicon ions injected into SiC. In 2017, Wang *et al.* used 35 keV silicon ions (Si^{2+}) to generate V_{Si} defect arrays with an efficiency of about 38% for single V_{Si} defects.[82] In 2022, He *et al.* used 30 keV He+ ions at a dose of 1×10^{13} cm^{-2} to generate V_{Si} with an efficiency of about 35%, achieving a spatial positioning accuracy of less than 60 nm in all three dimensions.[89] In 2024, He *et al.* utilized focused ion implantation to generate divacancies, where the linewidth of He^{+} induced defects ranged from 0.72–2.8 GHz, while C^{+} induced defects had linewidths ranging from 4.3–6.3 GHz,[91] this is explained by the lighter ions causing less damage to the lattice. Similarly, electron or neutron irradiation methods result in less lattice damage and narrower linewidths of around 100–200 MHz, superior to the linewidth produced by focused ion implantation.[24]

D. Laser writing

The laser writing method focuses a laser beam onto the SiC surface. The high energy of the laser causes local heating or excitation of the material, resulting in the introduction of defects and the generation of color centers. While the first three methods cause some lattice damage, laser writing can minimize it damage.[39,40] The defect type and concentration depend on the intensity and duration of the laser pulse, which can also produce defects at a specific depth in the crystal, with spatial resolution beyond the optical diffraction limit.[39,40] The 4H-SiC sample is mounted on a high-precision three-dimensional mechanical platform and translated along a preset trajectory during the laser writing process. By delivering a single pulse with a wavelength of 790 nm and a duration of 250 fs to each location in a 40×20 square grid, Chen *et al.* achieved positioning accuracy of about 80 nm in the transverse plane and generated a single V_{Si} defect with an efficiency of 30% in 2019.[64] In 2022, Almutairi *et al.* created a defect array using a 1030 nm femtosecond pulsed laser with a duration of 230 fs and a repetition rate of 200 kHz. The sample was annealed at 1000 °C in an argon atmosphere for 30 min. The positioning accuracy of VV^{0} center was about 200 nm.[92] In 2022, Day *et al.* demonstrated the fabrication of photonic cavity-integrated V_{Si} spin defects using a 337.1 nm nanosecond-pulsed laser, achieving an ODMR contrast of 0.15%.[93] In 2025, Hao *et al.* demonstrated the formation of defect arrays in 4H-SiC through femtosecond laser irradiation combined with thermal annealing.[94]

Table I summarizes the four methods for fabricating SiC spin defects, alongside other comparative parameters such as linewidth, spin coherence times, and optically detected magnetic resonance (ODMR) contrast. The fabrication method significantly influences the optical and spin properties of the defects. Suitable preparation methods and optimized process parameters are crucial depending on the specific application requirements. More efforts will focus on enhancing coherence times, improving defect uniformity, narrowing linewidth, and developing large-scale manufacturing techniques to advance SiC-based quantum technology technologies.[65,95,96]

III. SPIN AND PHOTONS OF SPIN DEFECTS IN SiC

A. Spins in SiC

Defect centers in SiC have garnered significant interest because of their well-defined spin states, which can be controlled using microwave fields and readout through photon counting. These spin states display long coherence times and high controllability at room and cryogenic temperatures.[18,96,97] Through optical and microwave manipulation, electron and nuclear spins in SiC can function as key components for fast quantum operations and quantum storage, respectively, facilitating the development of quantum registers and nodes.[98] This section will discuss the characteristics and manipulation techniques of electron and nuclear spins in SiC and their potential applications in quantum network technologies.

1. Electron spin

Quantum defect in SiC can form stable electron spin states, exhibiting long coherence times and high-fidelity quantum control.[18,99–102] Several critical conditions must be met to build efficient qubits or network nodes: long coherence times to ensure stable information storage, precise coherent control to enable quantum logic operations, and flexible device integration and operation. The following discussion focuses on spin coherence and charge control, offering deeper insights.

a. Spin coherence. Spin decoherence remains a substantial challenge in defect-based quantum information processing, predominantly arising from interactions between spins and their environment.[103] These interactions include lattice vibrations (phonons), dipole–dipole

TABLE I. Summary of different methods for fabricating spin defects in SiC.

Methods	Defect types	Ion species	Linewidth (MHz)	Spin relaxation time ($T_1/\mu s$)	Pure dephasing time ($T_2^*/\mu s$)	Spin coherence time ($T_2/\mu s$)	ODMR contrast (%)	Year
Electron or neutron irradiation	V_{Si}	e^-	61, 73	N.A.	1.68	11	N.A.	2024[25]
			N.A.	500	N.A.	N.A.	0.6	2015[17]
	Divacancy (PL1, 2, 4)	e^-	N.A.	N.A.	1.1–4.4	1200	9-15	2015[67]
	Ky5(3C-SiC)	e^-	2000	N.A.	0.2–1.8	901	N.A.	2017[24]
Ion implantation	V_{Si}	He^+	25–101	N.A.	34	1390	N.A.	2022[87]
		H^+	20.9–226	N.A.	N.A.	N.A.	N.A.	2022[87]
		He^+	N.A.	N.A.	0.168	N.A.	0.7	2019[69]
	Divacancy (PL6)	C^+	N.A.	149.1	0.463	23.2	23	2022[96]
			4300–6300	N.A.	0.73	72.5	N.A.	2024[91]
	Divacancy (PL5)	C^+	N.A.	N.A.	1.66	24	18	2022[96]
	N_CV_{Si}	N^+	N.A.	N.A.	1.1	17.1	0.11	2020[74]
	Vanadium	V	650–850	0.17–1.2	N.A.	N.A.	N.A.	2020[86]
Focused ion beam implantation	V_{Si}	H^+	N.A.	178	N.A.	42	0.8	2017[83]
	Divacancy (PL6)	He^+	720–2800	3.6×10^4	2.04–3.27	118.4–194.2	16	2024[91]
Laser writing	Divacancy (PL5)	N.A.	N.A.	28	0.18	1.65	8,12	2025[94]
	Divacancy (PL6)	N.A.	N.A.	53.37	0.3	1.69	7	2025[94]

interactions with neighboring spins, and charge noise, which degrade spin coherence and shorten quantum state storage times.[103] Compared to many other solid-state materials, defect spins in SiC demonstrate significantly longer coherence times,[18,99,104] often ranging from tens of microseconds to several milliseconds, which is crucial for effective quantum state manipulation. This advantage stems from SiC's wide bandgap and the reduced noise environment of its crystal lattice.

Researchers have employed a range of optimization techniques to further extend spin coherence times, including spin echo,[17,67,105] dynamical decoupling,[106] isotopic purification,[46] and Hamiltonian engineering.[107] These techniques aim to mitigate environmental interactions, thus improving the performance of quantum information processing. Spin echo effectively reduces decoherence caused by surrounding noise by compensating for phase drifts. As shown in Figs. 2(a) and 2(b), Hahn-echo spin coherence times reaching the millisecond scale have been achieved in defects such as the negatively charged silicon vacancy[17] (V_{Si}) and neutral VV^0 center[67] in 4H-SiC. Seo *et al.* experimentally demonstrated that the VV^0 center in 4H-SiC possess a Hahn-echo coherence time of 1.3 ms, attributed to the decoupling of heterogeneous nuclear spin baths (^{13}C and ^{29}Si) at moderate magnetic fields and the suppression of strongly coupled homonuclear spin pairs.[108] This ability to achieve long coherence times fundamentally originates from SiC's unique structural properties: its longer bond lengths compared to other defects and the natural alternation of Si and C atoms (forming Si–C–Si or C–Si–C sequences). This atomic arrangement inherently increases the physical separation between like nuclear spins, thereby suppressing dipolar coupling within the spin bath. Dynamical decoupling techniques, such as CPMG or XY sequences, further suppress the impact of slowly varying noise in more complex environments. A spin coherence time exceeding 20 ms by combining dynamical decoupling with spin locking technologies has been demonstrated with the silicon vacancy V2 center.[106] Alternatively, isotopic purification reduces nuclear spin noise by lowering the concentration of magnetic nuclei in the SiC crystal, thereby enhancing electron spin coherence. Li *et al.* experimentally demonstrated that a type of divacancy center in 4H-SiC, PL6, has high spin readout contrast (~30%) and photon count rate (150kcps) under ambient conditions,[96] which are comparable to nitrogen vacancy centers in diamond as shown in Fig. 2(c). Figure 2(d) shows that the Ramsey spin decoherence time of VV^0 center increased 40-fold after isotopic purification.[46] Anderson *et al.* reported single-spin T_2, which exceeds 5 s with pulsed dynamical decoupling sequences in an isotopically purified host material.[109] Hamiltonian engineering has also emerged as an effective strategy for enhancing spin coherence. In particular, Miao *et al.* demonstrated that the VV^0 center in 4H-SiC could be coherently driven by electric fields, allowing the tuning of the Hamiltonian to enhance coherence times, even in the presence of noise.[110] Moreover, Miao *et al.* showed that microwave dressing of spin states could create a decoherence-protected subspace (DPS), leading to a substantial increase in spin coherence time ($T_2^* > 22$ ms, $T_2 \approx 64$ ms) by protecting the system from magnetic and electric field fluctuations.[23] In addition, Onizhuk *et al.* explored the role of avoided crossings in solid-state qubits and showed that by carefully controlling the Hamiltonian at clock transitions, they could mitigate decoherence arising from the nuclear spin bath.[107]

b. Charge states. The spin coherence in SiC is influenced not only by the intrinsic properties of their spin states but also by the charge states of the defects. Both V_{Si} and VV^0 centers can exist in multiple charge states,[100,101] and the different charge states significantly influence spin coherence time, controllability, and coupling efficiency with external fields. By applying external electric fields[102] or controlling doping levels, the charge states of these defects can be precisely tuned.

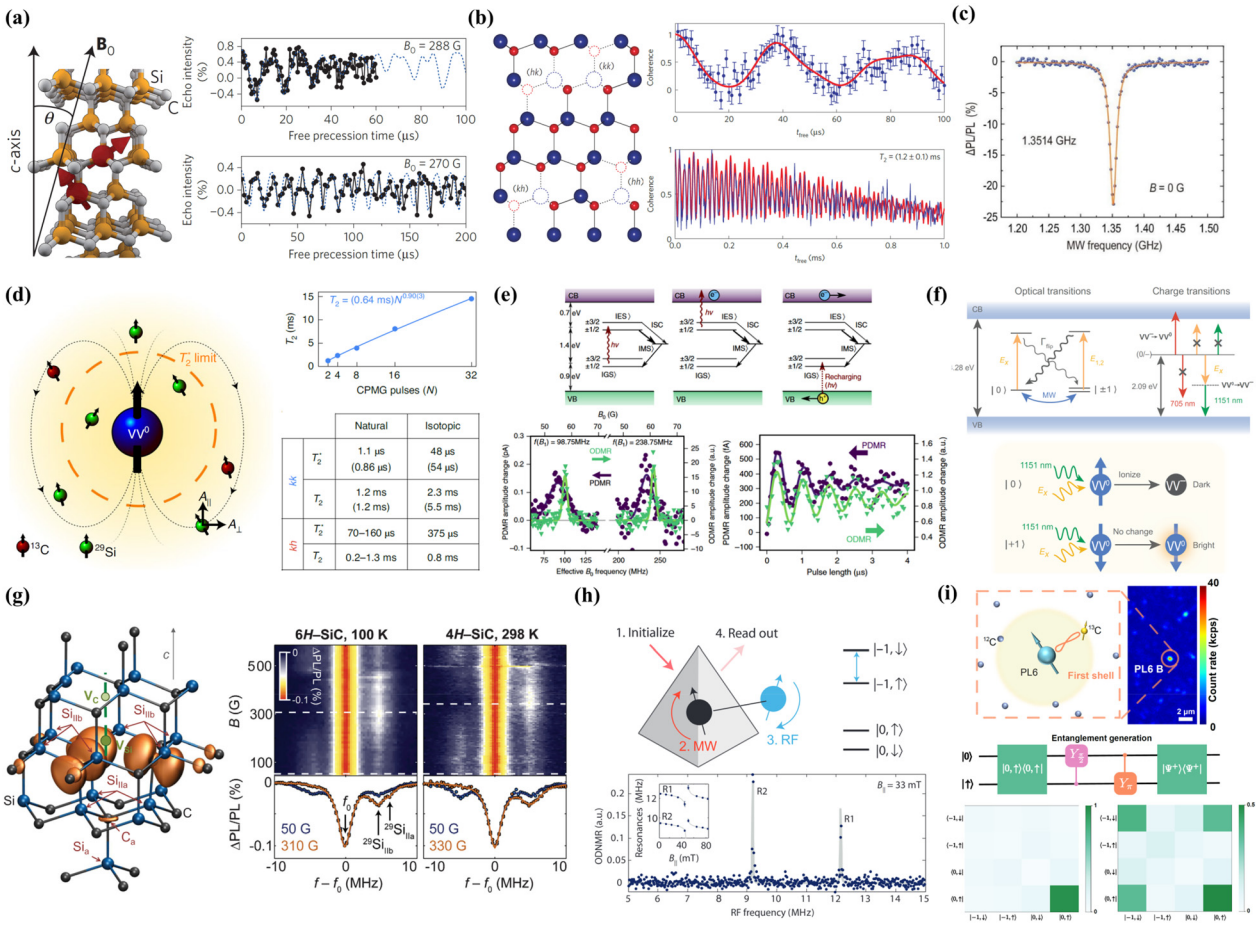

FIG. 2. Electron and nuclear spins in SiC. (a) Coherent control of a single V_{Si} in 4H-SiC. Left: Schematic of the 4H-SiC crystal structure with embedded silicon vacancy. Right: Hanh-echo decay of a single V_{Si} spin at external magnetic fields of $B_0 \approx 270$ and 288 G.[17] Reproduced with permission from Widmann *et al.*, Nat. Mater. **14**, 164–168 (2015). Copyright 2015 Springer Nature Limited. (b) Coherent control of a single VV^0 center in 4H-SiC. Left: Atomic structure of the VV^0 center in 4H-SiC, where h and k denote lattice sites. Right: Hanh-echo decay of a single kk divacancy center and kk divacancy ensemble (right).[67] Reproduced with permission from Christle *et al.*, Nat. Mater. **14**, 160–163 (2015). Copyright 2015 Springer Nature Limited. (c) ODMR measurements of a single PL6 divacancy center in 4H-SiC.[96] Reproduced with permission from Li *et al.*, Nat. Sci. Rev. **9**, nwab122 (2022). Copyright 2022 Oxford University Press. (d) Schematic of a single VV^0 center with surrounding nuclear spins. Top right: Coherence time (T_2) of a kk divacancy center in an isotopic sample with varying number of CPMG pulses N. Bottom right: T_2^* and T_2 for kk and kh defects in natural and isotopically enriched samples, respectively.[46] Reproduced with permission from Bourassa *et al.*, Nat. Mater. **19**, 1319 (2020). Copyright 2020 Springer Nature Limited. (e) Top: Charge dynamics of the V_{Si} photocurrent detected magnetic resonance (PDMR). Bottom left: Comparison of PDMR and optically detected magnetic resonance (ODMR) signals. Bottom right: Electrically detected Rabi oscillations contrasted with optically detected Rabi oscillations.[111] Reproduced with permission from Niethammer *et al.*, Nat. Commun. **10**, 5569 (2019). Copyright 2019 Springer Nature Limited. (f) Optical and charge transitions of the VV^0 center in 4H-SiC. Top: Energy level diagram illustrating optical and charge state transitions. Bottom: Schematic of spin-to-charge state mapping.[109] Reproduced with permission from Miao *et al.*, Sci. Adv. **8**, eabm5912 (2022). Copyright 2022 The American Association for the Advancement of Science. (g) VV^0 center in 6H-SiC and hyperfine interactions. Left: Atomic structure of a VV^0 center in 6H-SiC with nearby ^{29}Si nuclei at the Si_{IIa} and Si_{IIb} sites. Right: ODMR spectra of the (hh) divacancy center in 6H-SiC and PL6 in 4H-SiC with different magnetic fields. The ^{29}Si nuclei are polarized near the ESLAC points (B = 310 G and B = 330 G), respectively.[114] Reproduced with permission from Falk *et al.*, Phys. Rev. Lett. **114**, 247603 (2015). Copyright 2015 American Physical Society. (h) Top: Hybrid two-qubit quantum register comprising a PL6 electron spin and a proximal ^{29}Si nuclear spin. Bottom: Optically detected nuclear magnetic resonance (ODNMR) of the nuclear spin.[117] Reproduced with permission from Klimov *et al.*, Sci. Adv. **1**, e1501015 (2015). Copyright 2015 The American Association for the Advancement of Science. (i) Quantum register consists of a PL6 electron spin and a nearby first-shell ^{13}C spin. Nuclear spin initialization and electron-nuclear entanglement generation.[98] Reproduced with permission from Hu *et al.*, Nat. Commun. **15**, 10256 (2024). Copyright 2024 Springer Nature Limited.

Moreover, the spin-dependent intersystem crossing (ISC) enables efficient spin-to-current conversion. The spin state can only be read by detecting photocurrent, which is highly advantageous for scalable electrical integration. As shown in Fig. 2(e), the electrical readout of silicon vacancies (V_{Si}) center in 4H-SiC at room temperature was demonstrated, offering a comparison between photocurrent detected magnetic resonance (PDMR) and optically detected magnetic resonance (ODMR).[111] Furthermore, PDMR has been applied to electron-nuclear double resonance (PD-ENDOR), enabling room-temperature detection of ^{29}Si nuclear magnetic resonance.[112] This method can identify nuclear

spins coupled to the V2 center electron spins, laying the groundwork for developing electrically driven integrated quantum devices. In addition, by preparing spin states in specific charge states (e.g., stable states in low-charge-noise environments), coherence times can be effectively extended, enhancing quantum information storage capabilities. As shown in Fig. 2(f), divacancy centers' VV^0 and VV^- charge states correspond to bright and dark states, respectively.[109] The spin-to-charge conversion enables single-shot readout, demonstrating the potential for highly efficient quantum information processing. This flexible charge-state modulation endows SiC systems with compatibility across optical, microwave, and electrical interfaces, greatly expanding their applicability in quantum network technologies.

2. Nuclear spin

Nuclear spins in SiC, such as ^{13}C and ^{29}Si, are valuable quantum resources due to their long coherence times and potential for quantum memory applications in quantum networks, making them highly suitable for use as quantum memories.[99] Furthermore, the strong coupling between nuclear and electron spins enables them to create efficient quantum registers, facilitating the collaborative storage and processing of quantum information.

a. Nuclear spin initialization. High fidelity spin initialization is fundamental to quantum technologies and applications.[113] Initializing nuclear spins in SiC is a critical step to fully leverage their long coherence times and high stability for quantum storage and information processing. Dynamic nuclear polarization (DNP)[114,115] is one of the techniques for achieving efficient nuclear spin initialization. By utilizing the hyperfine interaction between electron spins and nuclear spins, DNP transfers the optically initialized electron spin polarization to nuclear spins, thereby achieving nuclear spin polarization. As shown in Fig. 2(g), strong coupling between the PL6 color center in 4H-SiC and the ^{29}Si nuclear spin, and between the VV^0 center in 6H-SiC and ^{29}Si, has enabled dynamic nuclear polarization near the exited states level anticrossing (ESLAC) point through optical pumping. This process achieves a polarization rate of 99% at room temperature, corresponding to an effective nuclear temperature of 5 μK.[114] Furthermore, theoretical studies have demonstrated that near-unity polarization via DNP is achievable even in weakly coupled electron-nuclear spin systems. Both theoretical and experimental results have shown that nuclear spin polarization can be reversed with a magnetic field change as small as 0.8 G.[116] This mechanism opens new avenues for DNP-based sensing and radio frequency-free control of nuclear qubits. Another DNP example is depicted in Fig. 2(h). After optical initialization of the PL6 electron spin ensemble in 4H-SiC, ^{29}Si nuclear spins, strongly coupled to PL6 centers, undergo dynamic nuclear polarization (DNP) via hyperfine interactions between the electron and nuclear spins, achieving a polarization rate of up to 99%. By applying a resonant radio frequency field, nuclear spins can be readout using optically detected nuclear magnetic resonance (ODNMR).[117]

b. Electron-nuclear entanglement. In scalable quantum networks, qubits are distributed across multiple nodes, with electron-nuclear spin entanglement serving as the fundamental building block for quantum nodes. The initial demonstration of electron-nuclear entanglement was achieved in isotopically engineered bulk silicon carbide (SiC) in 2020. Subsequently, within the SiC photonic platform [Fig. 2(i)], Hu *et al.* demonstrated near-unity (~100%) spin initialization of a single ^{13}C nuclear spin in SiC. Both the electron spin (PL6, a divacancy spin species in SiC) and the nuclear spin exhibit coherent controllability, enabling the preparation of a maximally entangled Bell state with 0.89 fidelity under ambient conditions.[98] Furthermore, the research team successfully integrated this spin register into a SiC photonic waveguide while preserving its intrinsic spin coherence and photon properties.

B. Photons in SiC

Ion implantation and ion irradiation cause lattice damage, resulting in a broader optical linewidth.[24,67,87,91] Furthermore, fluctuating charge noise significantly impacts the optical emission linewidth.[118] The ability to adjust the wavelength is another essential technique in quantum networks. Two nominally identical color centers are unlikely to have the same spectral frequency due to their sensitivity to surrounding electrostatic disturbances. This presents a significant challenge when trying to interfere with two remote defects.[119] This section will introduce techniques to narrow the linewidth and tune the wavelength of SiC color centers.

1. Wavelength tuning and linewidth reduction

Under an external electric field, the dipole term perturbs the ground and excited state energy levels of defects, resulting in a Stark shift.[118] Due to different group symmetries, color centers exhibit distinct electric dipole moments, leading to varying wavelength tunability under the same electric field. Bassett *et al.* demonstrated precise control over the ZPL transition of a single NV center diamond using a multi-axis electric field, achieving a frequency shift of over 10 GHz.[120] Guo *et al.* employed a metal-insulator-metal (MIM) structure to generate a 10^5 V/cm electric field near a single NV^0 center in diamond, observing significant wavelength shifts at low temperatures. They demonstrated the field dependence of the electrically driven emission and extracted the NV^0 ground state electric field susceptibility 15.83 GHz/mMV.[121] Day *et al.* demonstrated electrical control of G-center ensembles on SOI by combining a transverse p-i-n structure. Applying a reverse-biased DC electric field, they observed 100% fluorescence modulation and a wavelength redshift of 1.24 GHz/V.[122] These electric tuning demonstrations in diamond inspired the SiC quantum defects as well. On the SiC platform, as illustrated in Fig. 3(a), de las Casas *et al.* demonstrated the use of electric fields to tune the optical transition frequencies of VV^0 centers in 4H-SiC over a range of several GHz via the DC Stark shift, while stabilizing their charge states on microsecond timescales.[123] Rühl *et al.* used epitaxial graphene to fabricate transparent interdigital electrodes. They applied large electric fields in axial and radial directions, observing more than 3 meV Stark shifts in V_{Si} as depicted in Fig. 3(b).[124] Anderson *et al.* integrated a divacancy (VV^0) center with C_{3v} symmetry into a commercial vertical p-i-n structure, achieving the largest wavelength tuning to date, with a Stark shift of 850 GHz.[66] Moreover, they found the electric fields also caused charge depletion, leading to a dramatic narrowing of the transitions linewidth.

Advancing electric field control techniques to suppress charge noise and narrow linewidths to their natural limits has emerged as a pivotal strategy. Akbari *et al.* suppressed spectral diffusion in hexagonal boron nitride by applying an out-of-plane static electric field, reducing the linewidth by nearly two orders of magnitude,

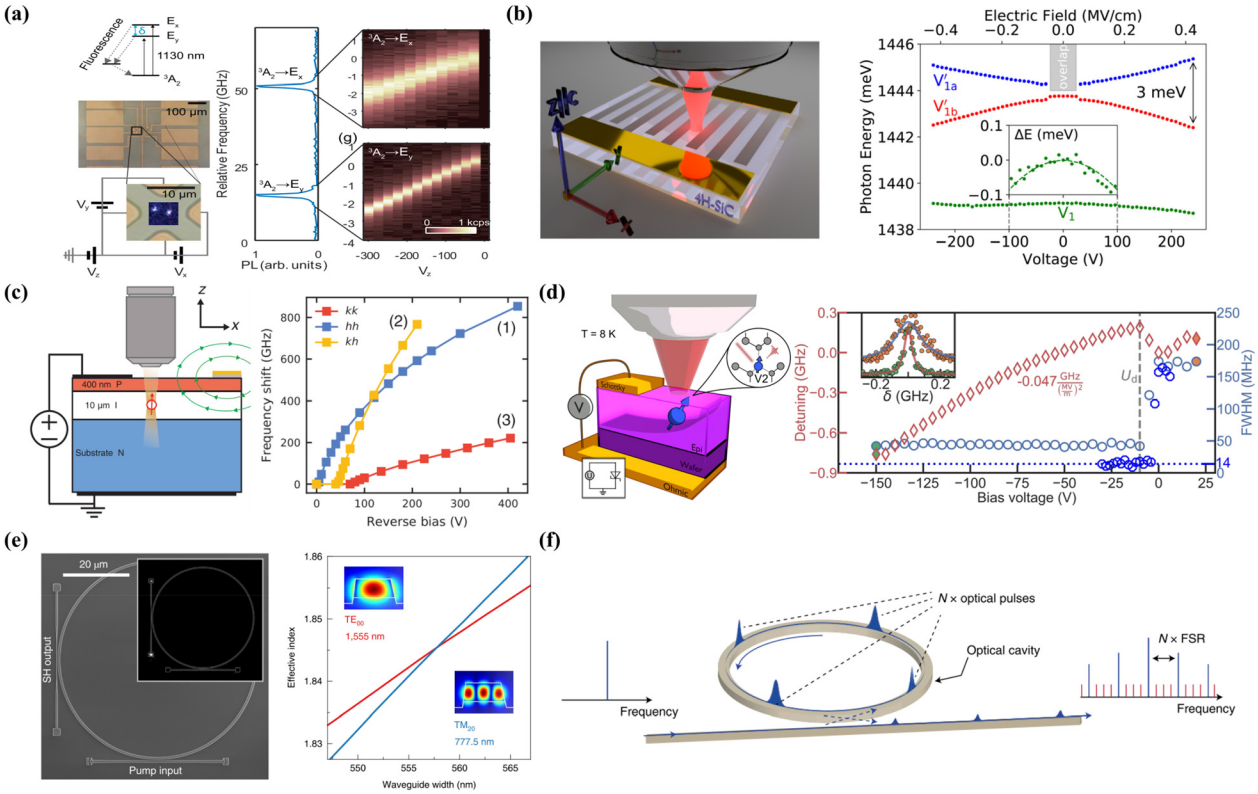

FIG. 3. Wavelength tuning and linewidth reduction. (a) DC Stark tuning of neutral VV^0 centers in 4H-SiC: Electric-field-induced GHz-scale optical transition frequency shifts with stabilized charge states under microsecond-scale control.[123] Reproduced from de las Casas *et al.*, Appl. Phys. Lett. **111**, 262403 (2017), with the permission of AIP Publishing. (b) Voltage-driven spectral tuning of V_{Si} centers: Direct electrical modulation achieves 3 meV Stark shift in V_{Si} defects.[124] Reproduced with permission from Rühl *et al.*, Nano Lett. **20**, 658–663 (2019). Copyright 2019 American Chemical Society. (c) Integrated p-i-n junction for VV^0 center control: These devices enable deterministic charge-state control and broad Stark shift tuning exceeding 850 GHz.[66] Reproduced with permission from Anderson *et al.*, Science **366**, 1225–1230 (2019). Copyright 2019 American Association for the Advancement of Science. (d) Schottky diode enabled V2 defect optimization: Charge carrier depletion suppresses spectral diffusion, yielding lifetime-limited linewidth and enhanced spin-photon entanglement fidelity.[126] Reprinted with permission from Steidl *et al.*, arXiv:2501.04583 (2025). (e) Second-harmonic generation (SHG) in SiCOI microring resonators: TE_{00} to TM_{20} mode conversion (1555 to 777.5 nm) and quadratic power dependence confirms 360%/W SHG efficiency.[27] Reproduced with permission from Lukin *et al.*, Nat. Photonics **14**, 330–334 (2020). Copyright 2020 Springer Nature Limited. (f) Soliton crystal-mediated frequency conversion: Kerr microresonator hosting a coherent soliton lattice (classical comb: blue; quantum comb: red).[29] Reproduced with permission from Guidry *et al.*, Nat. Photonics **16**, 52–58 (2021). Copyright 2021 Springer Nature Limited.

approaching the lifetime limit linewidth.[125] In 2019, Anderson *et al.* used a p-i-n junction to suppress charge noise around the VV^0 color center, achieving a linewidth of 20 MHz in the fitted spectrum, close to the lifetime-limit.[66] Figure 3(d) presents a Schottky diode in 4H-SiC by Steidl *et al.* to suppress charge noise and obtain a single V2 color center with a lifetime-limited linewidth.[126] Under depletion conditions, the system demonstrated 99.8% confidence in spin-photon entanglement, with the entanglement success rate increasing from 35% to 60.4%. This improvement significantly advances the development of quantum networks.

2. Wavelength conversion

Photons as flying qubits are essential for long-distance communication and distributed quantum computing in quantum information processing. However, the high transparency windows of quartz optical fibers are restricted to telecom wavelength bands of 1300 and 1550 nm. Quantum defects emit at varying wavelengths, with some falling within the telecom range wavelength.[77,127,128] V^{4+} in SiC have stable and narrow emission in the O-band (1278–1388 nm), making them ideal for low-loss optical fiber transmission in quantum networks.[70–73,86,129] Additionally, while the SiV center in diamond[130,131] has inversion symmetry that protects it from electric fields and strain, the V^{4+} defects in 4H-SiC do not possess this symmetry. Instead, their orbital degeneracy and Jahn-Teller manifold strongly couple to lattice distortions, making them highly strain-susceptible.[52,132] Strain can significantly impact quantum networks by suppressing decoherence, tuning the zero-phonon line (ZPL) wavelength for indistinguishability, and coupling different quantum systems. In addition to V^{4+} in SiC, most SiC defects are not in the telecom band, leading to significant losses in fiber transmission. This limitation has driven the development of quantum frequency conversion (QFC) technology. QFC devices utilize second-order nonlinear materials, such as periodically poled lithium niobate waveguides, where up to 86% single-stage conversion

efficiency has been achieved at the single-photon level.[133] Efficient frequency conversion has also been demonstrated on a monolithic platform with GaAs quantum dots,[55] although high photon losses in GaAs have limited its further development.[74] SiC is unique in combining quantum emitters,[77] strong second-order optical nonlinearity,[134,135] high thermal conductivity,[136] wide bandgap, and piezoelectric response,[137] making integrated quantum conversion and frequency conversion possible. In 2019, Song *et al.* successfully fabricated 4H-SiC photonic crystal nanocavities without hydrogen ion implantation, achieving frequency conversion in the telecom band with a second-harmonic conversion efficiency of 1900%/W.[138] This efficiency is the ratio of the second harmonic power generated in the output waveguide to the square of the pump power in the input waveguide. Figure 3(e) shows the work of Lukin *et al.* demonstrated efficient second-harmonic generation (SHG) in a high-Q microring resonator on the SiCOI platform, achieving SHG efficiency of 360%/W by designing phase matching between the quasi-TE mode at 1555 nm (TE00) and the quasi-TM mode at 777.5 nm (TM20) in 2020.[27] As shown in Fig. 3(f), Guidry *et al.* demonstrated that a stable temporal lattice of solitons could isolate a multimode below-threshold Gaussian state from any admixture of coherent light.[29] Although many experiments on the SiC platform have successfully leveraged its nonlinearity to achieve frequency conversion in the telecom band, a comprehensive demonstration of nonlinear optics in the telecom band,[139,140] combined with enhanced efficient quantum emitters on a monolithic platform, has yet to be realized. This will be one of the key achievements in future research.

IV. SPIN-PHOTON INTERFACE

In quantum networks, entanglement between stationary qubits (e.g., solid-state spins) and flying qubits (e.g., photons) is a crucial step, which can be achieved through frequency encoding[54] or polarization encoding:[53,141] frequency encoding maps non-degenerate spin states in a three-level system to distinct photon frequencies, while polarization encoding distinguishes degenerate spin states via photon polarization in three- or four-level systems. Quantum dots and diamond NV centers have made significant strides in spin-photon entanglement research, providing valuable insights for emerging materials like silicon carbide. Spin-photon entanglement has been demonstrated in quantum dots in 2012 via polarization or frequency encoding,[53,142] with improvements in entanglement fidelity through frequency conversion and telecom C-band emission.[54] Spin-photon entanglement in diamond has been demonstrated in 2010.[141] Time-encoded entanglement between photons and both electron and nuclear spins has also been reported.[55,143] In 2022, Stas *et al.* showcased a two-qubit node based on silicon-vacancy centers in diamond,[144] utilizing high-strain silicon-vacancy centers in nanophotonic cavities to achieve entanglement between electron-photon and nuclear spin-photon pairs. Additionally, they employed electron spins as flag qubits for error detection in nuclear spin-photon gates, offering a viable physical platform for scalable quantum repeaters. These successes in solid-state systems provide critical theoretical and experimental foundations for realizing spin-photon entanglement in silicon carbide.

A. Single-shot readout

High-fidelity readout is an essential component of spin–photon entanglement interfaces, particularly in single-shot readout techniques implemented in solid-state systems such as silicon carbide (SiC). These techniques enable rapid verification of spin-photon entanglement states through single measurements with high fidelity, minimizing quantum state perturbations caused by repeated measurements while enhancing the efficiency of entanglement generation and distribution. In 2024, Lai *et al.* achieved high-fidelity single-shot nuclear spin readout by developing an innovative approach utilizing 250 readout cycles.[145] Targeting the ^{29}Si nucleus adjacent to a silicon vacancy V2 center, their protocol [Fig. 4(a)] successfully discriminated between nuclear spin bright and dark states within a 1.13 ms measurement window through repeated CNOT operations and optical readout, attaining a fidelity of 98.2%. Furthermore, a refined two-step readout scheme enhanced the fidelity to 99.5% with 89.8% success efficiency. Concurrently, Hesselmeier *et al.* implemented a two-point measurement protocol [Fig. 4(b)] incorporating charge-resonance checks (CRC) to screen ionization events, achieving 92% standard readout fidelity for an ancillary ^{29}Si nuclear spin.[146] Post-selection further improved fidelity to 99.5%, albeit with a reduced success rate of 10%. Their work additionally demonstrated nuclear spin Rabi oscillations exhibiting 96% contrast, while photon-threshold-dependent fidelity analysis revealed performance limitations arising from elevated bright-state flip rates. Additionally, Anderson *et al.* demonstrated single-shot readout (SSR) through spin-to-charge conversion, achieving a fidelity of approximately 70%.[109]

B. Spin–photon interface in SiC

The experimental demonstration of time-bin encoded spin-photon entanglement in silicon carbide (SiC) was reported in 2024 as shown in Fig. 4(e).[25] The protocol begins with defect state preparation via resonant optical pumping, followed by microwave pulses to rotate the spin into a superposition state. Pulsed optical excitation is then applied to trigger photon emission, with subsequent photon collection. An additional microwave pulse combined with further pulsed optical excitation and photon collection completes the spin-photon entanglement generation process. Photon encoding is implemented based on their temporal arrival order at the detector. Finally, the spin state is reconstructed through microwave-assisted manipulation and excitation light-driven collection of phonon sideband signals, enabling experimental verification of the maximally entangled state. Crucially, Bell state verification requires demonstrating superposition-basis correlations that cannot be inferred exclusively from photon arrival timing statistics. To address this, the research team utilized a Pockels cell for time-to-polarization encoding conversion and implemented phase stabilization through a non-equilibrium interferometer. This configuration enabled superposition-basis readout of the spin state. By analyzing photon-spin correlation patterns, the experimentalists confirmed high-quality entanglement with a fidelity of 75.7%, significantly surpassing the 50% certification threshold.

V. SILICON CARBIDE INTEGRATED PHOTONICS

As discussed in Sec. IV, achieving spin-photon entanglement in defect centers of various material platforms such as quantum dots,[147–149] diamond,[55,144] and silicon carbide[25] requires strong light-matter interactions to enhance the entanglement generation rate. As the demands for SiC photonic devices in future quantum networks increase, the on-chip integration of SiC becomes crucial. Integrated quantum photonic circuits typically consist of quantum emitters or

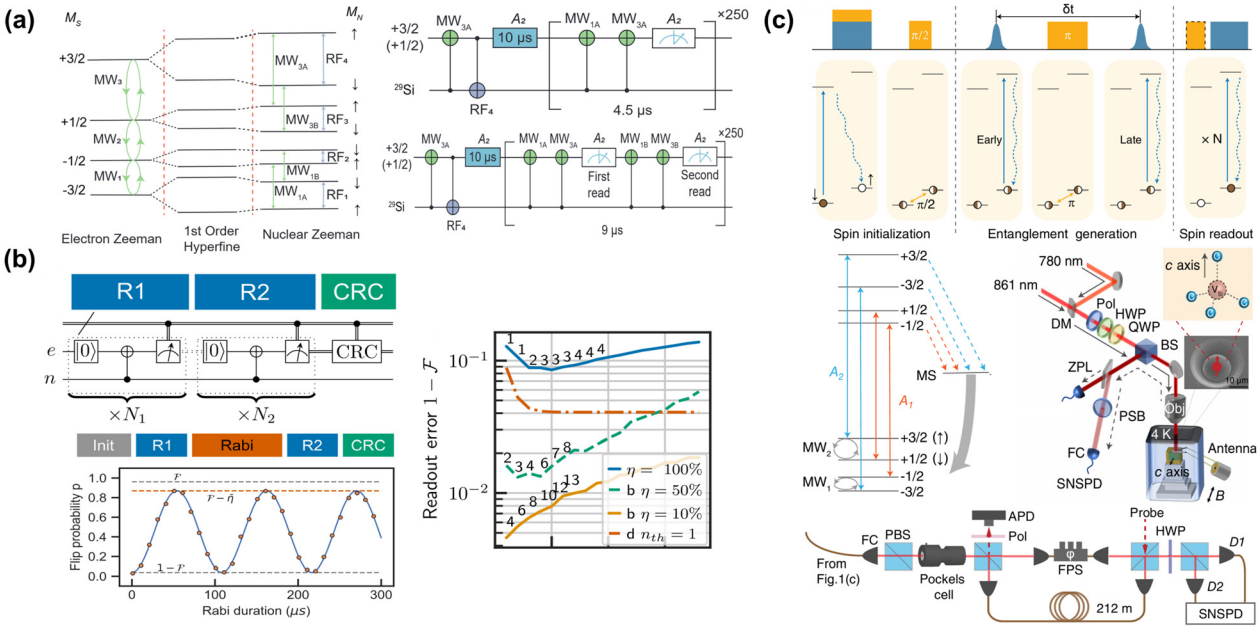

FIG. 4. Single-shot readout and spin-photon interface of silicon carbide. (a) Energy level diagram illustrating the coupling between a silicon vacancy V2 center and a ^{29}Si nuclear spin under an applied magnetic field, accompanied by two distinct single-shot nuclear spin readout methodologies.[145] Reproduced with permission from Lai *et al.*, Phys. Rev. Lett. **132**, 180803 (2024). Copyright 2024 American Physical Society. (b) Two-point measurement protocol comprising sequential readout steps (R1 and R2) integrated with charge-resonance check (CRC) for ionization event filtering. The nuclear spin Rabi oscillation measurement workflow involves initialization, R1 readout, variable-duration Rabi driving, R2 readout, and CRC validation. Corresponding readout error analysis for the two-point scheme is presented.[146] Reproduced with permission from Hesselmeier *et al.*, Phys. Rev. Lett. **132**, 180804 (2024). Copyright 2024 American Physical Society. (c) Time-bin encoded spin-photon entanglement in 4H-SiC. Top panel: Schematic workflow for spin initialization, photon emission, and entanglement verification. Middle panel: silicon vacancy V2 center energy structure with optical separation of zero-phonon line (ZPL) and phonon sideband (PSB) signals for spin-state detection and interferometric characterization. Bottom panel: Non-equilibrium interferometer design implementing Pockels-cell-mediated time-to-polarization conversion, demonstrating 75.7% entanglement fidelity through quantum state tomography.[25] Reproduced with permission from Fang *et al.*, Phys. Rev. Lett. **132**, 160801 (2024). Copyright 2024 American Physical Society.

spins, waveguides, beam splitters, modulators, and other components.[19,150] As a wide bandgap semiconductor, silicon carbide has been extensively used in industry, leading to mature fabrication processes for large-scale, high-quality SiC wafers. With its exceptional optical properties, SiC is increasingly emerging as an excellent CMOS-compatible photonic material platform.[21] This section will explore how integrated photonic technologies can be beneficial to SiC quantum networks.

A. Photon confinement techniques in SiC-based platforms

The commonly studied SiC wafers are either 3C-SiC hetero-epitaxially grown on Si substrates or 4H-SiC homoepitaxially grown on SiC substrates. Since the refractive index of the epitaxial layer does not exceed that of the substrate, effective in-plane light confinement cannot be directly achieved. Two primary approaches have been developed to achieve in-plane light confinement: undercut techniques and thin-film technologies. Undercut techniques were the predominant choice before the maturation of thin-film fabrication processes. However, devices fabricated using undercut techniques face challenges in large-scale integration due to the lack of low-index substrate support. Developing SiC-on-insulator (SiCOI) thin-film technology has made large-scale integration feasible. Despite the advantages of thin-film technology for integration, suspended devices fabricated using undercut techniques still achieve superior optical confinement. Therefore, specific devices constructed on SiCOI platforms utilize undercut methods to release parts of the substrate, mitigating substrate-induced optical losses.[27,151]

1. Undercut techniques

Undercut techniques involve removing the substrate beneath the epitaxial layer to create a suspended structure with an air-SiC-air refractive index distribution, which enables effective optical field confinement within the device layer. The main challenge is to release part of the Si or SiC substrate without compromising the integrity of the device. For 3C-SiC on Si substrates, selective chemical etching can release the silicon substrate. In 2014, Lu *et al.* demonstrated suspended microdisk resonators with an intrinsic Q of 5.12×10^4 using this method,[152] as displayed in Fig. 5(a). For bulk 4H-SiC, surface doping followed by SiC epitaxial growth enables selective electrochemical etching of doped SiC layers, leaving the topmost device layer intact. This method, developed by Bracher *et al.*, has produced suspended nanobeam cavities with Q factors exceeding 7000,[153] though significant losses arise from the doping. Additionally, for 4H-SiC, angled reactive ion etching (RIE) can create suspended structures with triangular cross

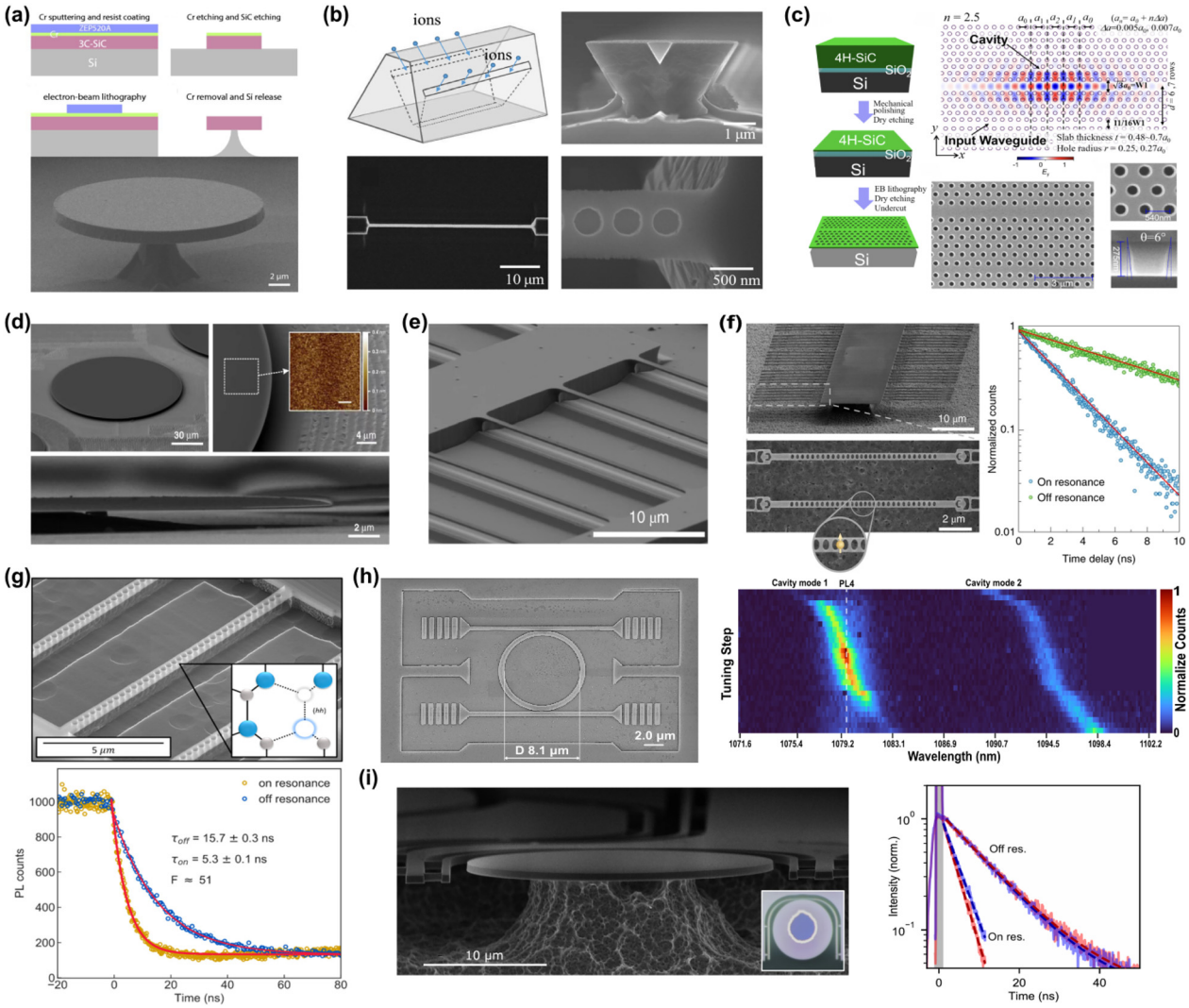

FIG. 5. Integrated quantum photonic devices with silicon carbide. (a) Suspended microdisk fabrication on 3C-SiC. Top: Process flow diagram for suspended microdisk fabrication. Bottom: SEM image of a 3C-SiC microdisk resonator achieving high-Q optical confinement.[152] Reproduced from Lu *et al.*, Appl. Phys. Lett. **104**, 181103 (2014), with the permission of AIP Publishing. (b) Nanobeam engineering via oblique etching. Schematic of ion-sheath control plate for angled etching. Scanning Electron Microscopy (SEM) image of a suspended nanobeam structure on bulk 4H-SiC with subwavelength mode confinement.[154] Reproduced from Song *et al.*, Appl. Phys. Lett. **113**, 231106 (2018), with the permission of AIP Publishing. (c) 2D photonic crystal cavity on 4H-SiCOI. Left: Fabrication workflow for 2D photonic crystal cavities on the 4H-SiCOI platform. Right: SEM image of the final cavity structure demonstrating optimized optical confinement.[138] Reproduced with permission from Song *et al.*, Optica **6**, 991–995 (2019). Copyright 2019 OSA Publishing. (d) High-Q microdisk resonator on 4H-SiCOI. SEM image of a fabricated microdisk resonator with an intrinsic Q of 7.1×10^6 on 4H-SiCOI.[151] (e) Low-loss waveguide with single SiC defects integration. Top: SEM image of inverted triangular waveguide integrated with V_{Si}).[87] Reproduced with permission from Babin *et al.*, Nat. Mater. **21**, 67–73 (2022). Copyright 2022 Springer Nature Limited. (f) Nanobeam cavity array and V_{Si} defects integration. Left: SEM of suspended nanobeam cavity array and zoomed-in view of the cavity. Right: Lifetime measurements with the cavity on and off resonance. Fitted lifetimes are $\tau_{off} = 6.66$ ns and $\tau_{on} = 2.45$ ns.[27] Reproduced with permission from Lukin *et al.*, Nat. Photonics **14**, 330–334 (2020). Copyright 2020 Springer Nature Limited. (g) Single VV^0 center coupled with photonic crystal nanobeam cavities. Top: SEM of nanobeam cavities and spatial PL mapping under resonant/non-resonant excitation. Bottom: Emission spectra with/without cavity enhancement and lifetime reduction measurements revealing a Purcell factor of 51.[162] Reproduced with permission from Crook *et al.*, Nano Lett. **20**, 3427–3434 (2020). Copyright 2020 American Chemical Society. (h) Gas-tuned microring cavity integrated with SiC ensemble defects. Left: SEM image of the microring cavity with a diameter of 8.1 μm. Right: The intensity map shows the redshift of the cavity mode as nitrogen gas is continuously injected.[164] Reproduced with permission from Bao *et al.*, ACS Photonics **12**, 2988–2996 (2025). Copyright 2025 American Chemical Society. (i) Two-emitter cavity quantum electrodynamics in 4H-SiCOI. Left: Integrated microdisk-waveguide architecture. Main: Scanning electron micrograph of a high-Q microdisk resonator coupled to a wrapping waveguide. Inset: Optical microscope image showing waveguide-disk coupling geometry with objective-based fiber coupling at waveguide facets. Right: Resonant coupling dynamics lifetime measurements for emitter A (blue) and emitter B (red) under on-resonance (solid) and off resonance (dashed) cavity conditions, demonstrating Purcell-enhanced emission dynamics.[26] Reproduced with permission from Lukin *et al.*, Phys. Rev. X **13**, 011005 (2023). Copyright 2023 American Physical Society.

sections. Song *et al.*[154] achieved suspended nanobeam cavities with Q factors up to 4×10^4 using this approach, as shown in Fig. 5(b).

2. SiC on insulator

This approach utilizes state-of-the-art SiC thin-film fabrication techniques to create SiC on insulator (SiCOI) structures. The resulting refractive index distribution enables robust optical confinement, eliminating the need for suspended architectures. Two leading methodologies have been developed for SiCOI fabrication: ion-cut technology and bonding-and-thinning technology. The ion-cut technique, developed in the 1990s and known as the Smart-cut process,[155] was initially used for silicon-on-insulator (SOI) fabrication. The process for SiCOI fabrication has matured significantly over the years. The fabrication sequence involves implanting hydrogen (H^+) or helium (He^+) ions into bulk 4H-SiC to create a splitting defect layer at a specific depth, followed by wafer bonding to a SiO_2-Si substrate. High-temperature annealing then separates the bulk 4H-SiC, leaving a 4H-SiC film on the SiO_2-Si substrate to form the 4H-SiCOI structure. This technique produces wafer-scale 4H-SiC films on SiO_2-Si substrates with uniform thickness and good surface roughness.[21] WGM optical microresonators fabricated on this platform have demonstrated Q factors around 7×10^4.[156,157] The primary Q-factor limitation stems from implantation-induced defects that cause optical scattering and absorption.

However, the smart-cut process damages the SiC lattice and generates many unwanted defects, making it challenging to isolate individual SiC defects. This limitation has sparked the development of the second method. The bonding-and-thinning approach eliminates the ion implantation-splitting step to minimize implantation-induced defects. Instead, bulk SiC is directly bonded to a SiO_2-Si substrate and mechanically thinned to achieve the desired film thickness. This method does not reuse bulk SiC and incurs higher costs due to the extreme hardness of SiC, which necessitates sophisticated thinning processes. However, it has gained significant interest for preserving the excellent properties of bulk SiC without introducing additional lattice defects. In 2019, Fan *et al.* demonstrated microdisk resonators with Q factors up to 2.42×10^5 using 3C-SiCOI obtained through bonding and thinning of epitaxial 3C-SiC on Si.[158] In the same year, Song *et al.* achieved photonic crystal cavities with Q factors reaching 6.3×10^5 using 4H-SiCOI [Fig. 5(c)].[138] In 2021, Wang *et al.*[151] further advanced the field by fabricating microdisk resonators on 4H-SiCOI and partially removing the underlying silica substrate[151] [Fig. 5(d)], achieving an intrinsic Q of 7.1×10^6, using these devices, broadband frequency conversions, including second-, third-, and fourth-harmonic generations have been observed.[151] These results indicate that when cost and processing efficiency are not primary concerns, wafer bonding and thinning represent the optimal approach for fabricating ultra-low-loss photonic devices on SiCOI platforms.

Undercut techniques enable strong optical confinement through suspended air-SiC structures, which are ideal for high-Q devices but suffer from mechanical fragility and limited scalability. SiCOI platforms, which integrate SiC films on low-index substrates, offer robust wafer-scale integration compatible with semiconductor workflows. While undercut excels in performance for specialized devices, SiCOI prioritizes scalable production despite higher costs and defect risks.

B. SiC integrated photonic devices

As discussed earlier, techniques such as device layer suspension by undercut and SiCOI thin-film fabrication enable effective in-plane light confinement, which forms a critical foundation for designing high-performance photonic devices. Using these optical confinement mechanisms, SiC-based photonic integrated circuits (PICs) can achieve efficient light manipulation and transmission through their key components, such as low-loss waveguides and high-Q resonators with small mode volume. A central focus in SiC quantum photonics is the coupling of color centers to these devices, facilitating strong light-matter interactions. In Table II, we summarize the performance of various microcavities on different SiC platforms.

1. Waveguide

A waveguide is a physical structure that guides electromagnetic waves from one point to another, confining and directing their propagation along a specific path while preventing energy dispersion into

TABLE II. Cavities engineered on different SiC platforms.

Platform	Resonator type	Photon confinement	Q factor	λ_{res}/nm	Spin integrated?	Purcell factor	Year
3C-SiC on Si	Microdisk	Suspended	5.1×10^4	1551	No	⋯	2014[152]
Bulk 4H-SiC	1D PhC	Suspended	4.0×10^4	1509	No	⋯	2018[154]
Bulk 4H-SiC	1D PhC	Suspended	5.1×10^3	1079	Divacancy	51	2020[162]
Bulk 4H-SiC	1D PhC	Suspended	2.7×10^3	859	V_{Si}	9.15	2021[163]
Bulk 4H-SiC	FP cavity	On substrate	7.4×10^4	917	V_{Si}	13.3	2025[167]
4H-SiCOI by ion-cut	Microring	On substrate	7.3×10^4	1549	No	⋯	2019[156]
3C-SiCOI by b&t[a]	Microdisk	On substrate	2.4×10^5	1581	No	⋯	2019[158]
4H-SiCOI by b&t	2D PhC	On substrate	6.3×10^5	1514	No	⋯	2019[138]
4H-SiCOI by b&t	Microdisk	Suspended	7.1×10^6	1561	No	⋯	2021[161]
4H-SiCOI by b&t	1D PhC	Suspended	1.5×10^4	859	V_{Si}	>9	2020[27]
4H-SiCOI by b&t	Microring	On substrate	1.3×10^3	1035	Divacancy	5	2024[164]
4H-SiCOI by b&t	Microdisk	Suspended	1.3×10^5	916	V_{Si}	39	2023[26]

[a]b&t, bonding and thinning.

undesired directions. Waveguides based on total internal reflection are used to route photons on-chip in a theoretically lossless and experimentally practical manner, requiring efficient coupling of color center emission into the waveguide. In 2022, Babin *et al.* fabricated a series of inverted triangular waveguides with a 45° opening angle in 4H-SiC. For a waveguide width of 500 nm, they achieved a high coupling efficiency of 82% (41% per propagation direction). Integrating bright single V2 color centers via He^+ implantation into a waveguide with 30% coupling efficiency and demonstrating nearly lifetime-limited photon emission and long spin coherence times, as shown in Fig. 5(e). Additionally, they achieved coherent control of a single nuclear spin near a V_{Si} center in the waveguide, realizing high-fidelity quantum gates.[87] In 2024, Hu *et al.* demonstrated the integration of the electron-nuclear entangled quantum register to the waveguide without compromising its entanglement fidelity.[98]

2. SiC photonic cavities

Building upon the SiCOI platform's advanced fabrication techniques, researchers improved the photon collection from single color centers by coupling quantum emitters to solid immersion lenses (SILs)[17,159] or nanopillars.[160,161] While these approaches enhance collection efficiency, they primarily focus on extracting emitted photons rather than engineering the emitter's intrinsic properties. To achieve the strong light-matter interactions required for scalable quantum networks, the integration of SiC photonic cavities becomes essential. Such cavities enable efficient light confinement and Purcell enhancement—critical for spin-photon interface establishment.

3. Photonic crystal cavity

Photonic crystals (PhCs) have periodic structures on the scale of optical wavelengths, creating bandgaps that prevent the propagation of certain wavelengths. Nanophotonic crystal cavities leverage this periodicity to confine light, making them vital components in advanced photonic devices like lasers, sensors, and quantum optical systems. In 2015, Bracher *et al.* fabricated the first suspended one-dimensional photonic crystal cavities in 4H-SiC, achieving a Q-factor of 7000. By tuning the cavity mode to couple with the zero-phonon line (ZPL) of silicon vacancy centers (V2), they enhanced the ZPL intensity by a factor of three.[153] In 2020, Lukin *et al.* further advanced this by fabricating suspended one-dimensional photonic crystal cavities on 4H-SiCOI with a Q-factor of up to 14 900. They observed a threefold reduction in emitter lifetime, demonstrating the potential of on-chip SiC thin films for high-performance quantum systems.[27] Additionally, Crook *et al.* demonstrated coupling of a suspended photonic crystal cavity on 4H-SiC with a neutral VV^0 center, achieving a threefold reduction in lifetime and an increase in the Debye–Waller factor from 5% to 75%, corresponding to a Purcell factor of 51, as depicted in Fig. 5(g).[162] However, they found that the coherence significantly deteriorated compared to that in bulk SiC, which they attributed to magnetic dipole interactions with electron spins from n-type dopants and surface charge traps. In 2021, Gadalaa demonstrated the enhancement of optical emission from photonic crystal cavities in silicon carbide (SiC) through below-bandgap irradiation and thermal annealing. The processes, including 785 and 532 nm irradiation and thermal annealing at 100 °C, improve defect–cavity interactions by modifying defect charge states and generating additional "bright states."[163]

4. Microring cavity

A microring cavity is a circular waveguide where light circulates due to constructive interference, with its resonant wavelength determined by the microring's circumference and the material's refractive index. Microring cavities are essential in integrated photonics for applications like optical communication, sensors, and quantum computing. In 2024, Bao *et al.* fabricated microring resonators on scalable 4H-SiCOI, observing a 36-fold enhancement in ZPL intensity and a Purcell factor of approximately 5.0.[164] The microring's filtering function also doubled the ODMR contrast of the PL4 spin, as displayed in Fig. 5(h).

5. Microdisk cavity

Microdisk cavities function similarly to microring cavities, utilizing whispering gallery modes (WGMs) formed by light undergoing multiple internal reflections along the disk's edge. These cavities are critical in integrated photonics, sensors, and quantum optics. In 2023, Lukin *et al.* fabricated suspended microdisk resonators on 4H-SiCOI with a Q-factor of up to 1.3×10^5. They integrated a pair of V_{Si} centers into the same microdisk cavity, achieving a cooperativity of 0.8 and observing dipole-induced transparency (DIT) in SiC.[26] Their results showed resonant lifetimes of 4.2 and 3.5 ns, with Purcell factors of 30 and 39, respectively. Furthermore, they demonstrated super-radiant emission from the two color centers coupled to the same cavity mode [Fig. 5(i)], opening new possibilities in quantum information processing.

6. Bullseye cavity

Bullseye cavities feature concentric rings that create periodic variations in refractive index, leading to specific resonances where light is strongly confined. These cavities are ideal for biosensing, lasing, quantum optics, and integrated photonics applications. In 2015, Li *et al.*[165] fabricated bullseye cavities on diamond thin films, achieving a record photon collection rate of 4.56 Mcps from a single NV center under saturation. In 2024, Barbiero *et al.*[166] coupled a single quantum dot emitting in the telecom O-band to an elliptical bullseye resonator, achieving broadband polarization-selective enhancement. The quantum dot exhibited a polarization degree of 96%, a threefold reduction in lifetime, and a Purcell factor of 3.9, with count rates as high as 3 MHz. They also demonstrated two-photon interference without external polarization filtering, showcasing the potential of bullseye cavities in enhancing light-matter interactions.

7. Fabry–Pérot cavity

FP cavity, with tunable spectral and spatial resonances, enhances light-matter interactions via high-finesse photon confinement. In 2025, Hessenauer *et al.* integrated silicon vacancy (V2) centers in 4H-SiC membranes into a fiber-based FP microcavity, achieving a 13.3-fold ZPL photon enhancement through Purcell effects and reduced emitter lifetime (7.3 to 5.6 ns).[167] This work underscores FP cavities as scalable spin-photon interfaces, with prospects for higher lifetime reduction via optimized coatings and integrated spin control for quantum networks.

Fabrication imperfections, such as surface roughness and sidewall irregularities, often result in photonic cavities with Q-factors lower

than theoretical predictions, primarily due to scattering losses and parasitic absorption. In 2023, Michaels *et al.* demonstrated plasma-based atomic layer etching (ALE) on 4H-SiC, achieving atomically smooth surfaces with subangstrom roughness. This ALE method reduces scattering losses, demonstrating the potential to significantly enhance Q-factors.[168] Following the advancements in SiCOI platform fabrication, the integration of SiC photonic cavities enhances light confinement and enables strong light-matter interaction, crucial for the development of efficient quantum devices. By embedding color centers into nanophotonic cavities or utilizing waveguide structures, the performance and scalability of SiC-based photonic systems can be significantly improved, paving the way for high-fidelity quantum information processing. These innovations in SiC photonics provide the foundation for scalable and integrated quantum technologies with advanced quantum communication, sensing, and computing capabilities.

VI. COLOR CENTER-BASED QUANTUM NETWORKS

Silicon carbide (SiC) offers unique advantages for quantum networks, such as long spin coherence times, telecom-compatible photon emission (e.g., V^{4+} defects), and the ability for CMOS integration. However, experimental progress in SiC-based multi-node entanglement is still in its early stages. In contrast, NV centers and V_{Si} centers in diamond have undergone decades of research and achieved significant milestones in quantum teleportation, repeaters, and fault-tolerant protocols. These breakthroughs or proposals involving diamond platforms provide essential technical roadmaps for SiC. This chapter focuses on how diamond-inspired architectures can guide the development of SiC's quantum network. We systematically analyze the breakthroughs in diamond's quantum networks and outline their adaptation pathways for SiC-based networks, given its unique material properties.

A. Quantum teleportation: Enabling reliable quantum state transfer

Quantum teleportation[169] provides a solution to the reliable transfer of quantum states between distant locations, addressing a significant challenge in quantum networks. By utilizing long-lived qubits at remote nodes, quantum state transfer can extend quantum key distribution (QKD)[170] over long distances, facilitating advancements in cloud-based quantum computing. However, direct transmission of quantum states via photon carriers is inherently unreliable due to transmission losses, and the no-cloning theorem prohibits creating multiple copies to counteract these losses. Quantum teleportation overcomes this issue by leveraging entanglement, allowing quantum states to be faithfully transferred between parties—Alice and Bob—once they share an entangled pair. This process is crucial for the development of quantum networks. In 2013, Bernien *et al.* established heralded entanglement between the electron spins of diamond NV centers, separated by three meters.[31] They encoded the quantum state to be transmitted onto the nuclear spin of one of the electron spins. By performing Bell-state measurements and employing real-time feedforward, they ensured successful quantum teleportation each time, with an average fidelity exceeding the classical limit.[35] This breakthrough demonstrated a key step in long-distance quantum communication. Further advancements in this field included demonstrating quantum teleportation by Hermans *et al.* in 2022 between non-adjacent nodes using entanglement swapping at an intermediate node and storing the quantum state in a storage qubit,[32] as depicted in Fig. 6(a). These developments have opened the door to more complex quantum networks. Additionally, quantum memories based on atomic-like systems have seen rapid progress.[171,172] If electron spins in NV centers can be coupled with other physical systems, it could enable higher fidelity entanglement and significantly enhance the scalability of quantum networks. In 2024, Iuliano *et al.* photon entanglement between diamond NV centers and photons suitable for thulium and rubidium quantum memories by using low-noise quantum frequency conversion and waveform shaping to align the temporal and spectral profiles of the photons. This achievement further underscores the growing potential of SiC in quantum network applications.[34]

B. Quantum repeaters: Overcoming distance limitations in quantum communication

Although quantum teleportation can bypass the no-cloning theorem to achieve long-distance communication, the rate of entanglement generation is still limited by the distance between the two nodes, specifically by the rate of distributing entangled qubits.[36,173] Briegel *et al.* proposed a quantum repeater protocol in 1998 to address this issue.[38] This method enables the establishment of long-distance entanglement that scales polynomially with time by using a series of intermediate nodes and nested purification protocols. The approach primarily relies on three key technologies:

First, heralded entanglement must be established between the nodes to suppress loss errors.[38,173] Over the past decade, this technique has been extensively developed in solid-state color center systems. In 2012, Bernien *et al.* accomplished two-photon interference with up to 66% contrast between two independent NV centers.[174] Shortly thereafter, Sipahigil *et al.* completed Hong-Ou-Mandel (HOM) interference for silicon vacancies at 5 K, providing the foundation for subsequent heralded entanglement experiments.[131] In 2013, Barrett *et al.*, following the protocol in Ref. 175, used single-photon joint measurements to predictively observe entanglement between diamond NV centers separated by three meters.[31] By employing techniques such as dynamic decoupling, charge state control, and spectral diffusion suppression, they achieved an entanglement generation rate of 39 Hz and a loss rate of 5 Hz in diamond NV centers, ultimately producing entanglement with a fidelity larger than 0.5 within a 100 ms cycle.[176] In 2024, Stolk *et al.* demonstrated heralded entanglement between two independently operating quantum nodes over a 10 km distance, as shown in Fig. 6(b). This was achieved by converting photons to the L-band for communication and embedding the link in a scalable, phase-stable architecture.[177] By fully utilizing the predictive capability of the network, along with real-time feedback logic for long-lifetime qubits, they ensured the successful distribution of heralded entanglement, regardless of the mode. In addition to the NV defects in diamond, Knaut *et al.* made significant advancements in the study of silicon-vacancy (V_{Si}) defects. As shown in Fig. 6(c), they coupled silicon vacancies into a diamond nanocavity to form a network node, enabling entanglement generation at a rate of 1 Hz between spatially separated quantum nodes. Furthermore, by leveraging the strong light-matter interaction provided by the cavity, they also demonstrated entanglement between nuclear spins through 40 km spools of low-loss fiber and a 35 km long fiber loop deployed in the Boston area urban environment.[59]

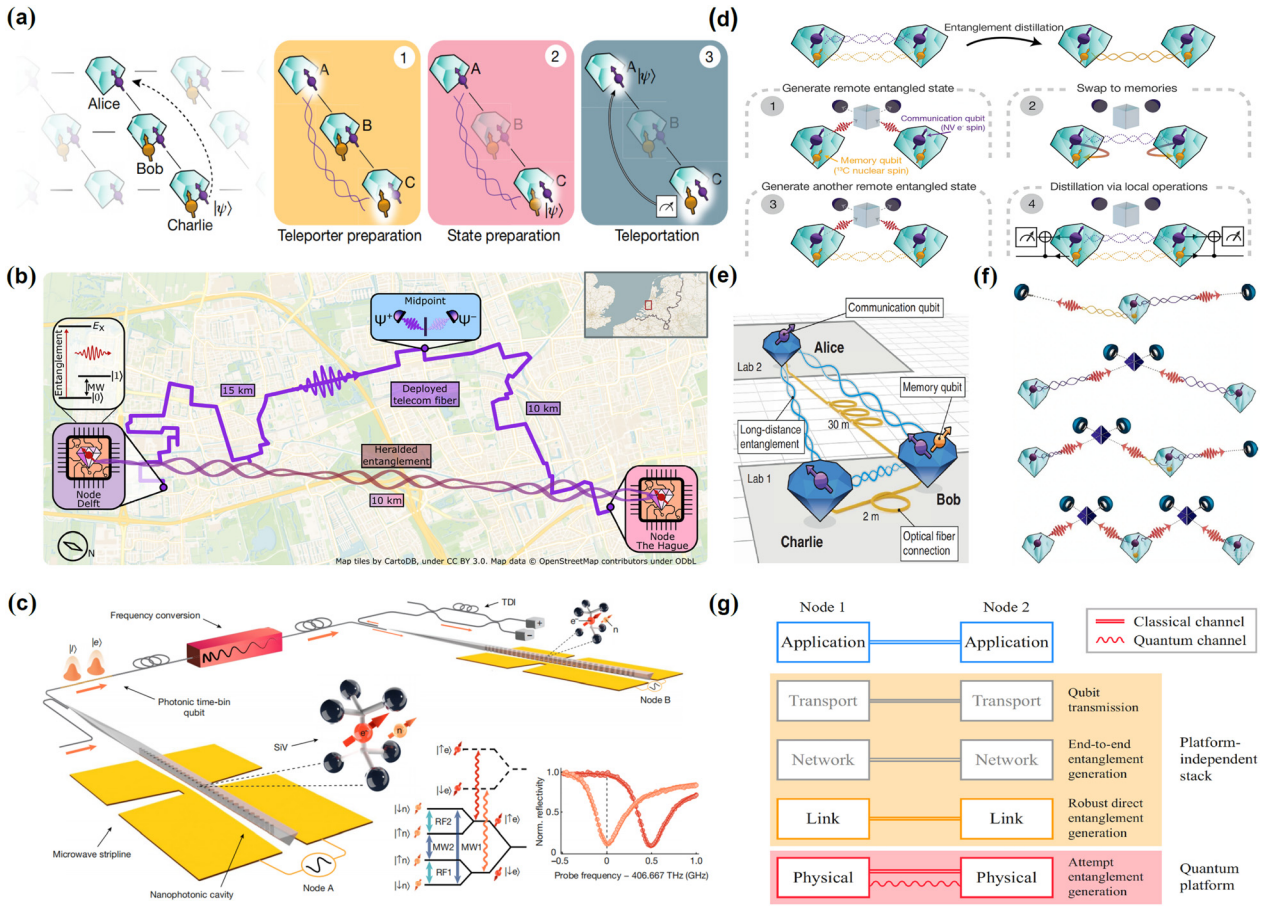

FIG. 6. Quantum network construction with diamond defects. (a) Teleporting a qubit between non-neighboring nodes of a quantum network. Non-adjacent node quantum teleportation protocol. Schematic of entanglement-mediated state transfer between distant nodes (A and C) via intermediate node B: Entanglement swapping between A-B and B-C links, quantum state encoding on nuclear spin at node C and Bell-state measurement-enabled teleportation to node A via classical channel. Key innovation: Real-time feed-forward operation achieving fidelity surpassing classical limits.[32] Reproduced with permission from Bernien *et al.*, Nature **497**, 86–90 (2013). Copyright 2013 Springer Nature Limited. (b) Heralded entanglement between two independently operating NV center quantum nodes over a 10 km distance with a signaling station.[177] Reproduced with permission from Stolk *et al.*, Sci. Adv. **10**, eadp6442 (2024). Copyright 2024 The American Association for the Advancement of Science. (c) Cavity-enhanced dual-node quantum interface. Top: Solid-state defect nodes (SiV center in diamond with nearby nuclear spins) coupled via photonic cavity. Bottom right: Hybrid control scheme combining microwave (blue), radio frequency (green), and spin-selective optical transitions (yellow/red). The reflection spectrum (curve) shows maximum contrast (dashed line) for spin readout and entanglement.[59] Reproduced with permission from Niu *et al.*, Nature **616**, 50–55 (2023). Copyright 2023 Springer Nature Limited. (d) Diagram of the entanglement purification principle in a quantum network, with steps 1–4 representing the specific stages of purification.[40] Reproduced with permission from Kalb *et al.*, Science **356**, 928–932 (2017). Copyright 2017 The American Association for the Advancement of Science. (e) The layout of a three-node quantum network, where optical fibers connect nodes to ensure entanglement generation. Long-distance entanglement is enabled through the intermediate node, Bob, and quantum state sharing is achieved via local operations.[33] Reproduced with permission from Pompili *et al.*, npj Quantum Inf. **8**, 121 (2022). Copyright 2022 Springer Nature Limited. (f) Diagrams of four types of quantum repeaters, from top to bottom: Single-sequence quantum repeater (SiSQuaRe) scheme, single-photon scheme, single-photon scheme with additional detection devices (SPADS), and dual-link single-photon scheme (SPOTL).[181] Reproduced with permission from Rozpędek *et al.*, Phys. Rev. A **99**, 052330 (2019). Copyright 2019 American Physical Society. (g) Quantum network stack architecture proposed by Pompili *et al.*[184] Reproduced with permission from Pompili *et al.*, NPJ Quantum Inf. **8**, 121 (2022). Copyright 2022 Springer Nature Limited.

Second, heralded entanglement purification[178,179] was employed to reduce operational errors. In 2017, Kalb *et al.* demonstrated this protocol, as shown in Fig. 6(d). They relied on a two-qubit node composed of electron and nuclear spins, which generated two entangled copies via heralded entanglement and entanglement swapping within the node. After applying local two-qubit gates, they used local operations to purify a high-fidelity entanglement from multiple low-quality entanglements, thus generating high-fidelity entanglement.[40]

The third approach is to extend nearby entanglements to remote nodes using entanglement swapping. In 2021, Pompili *et al.* integrated remote quantum nodes based on diamond communication qubits into a scalable phase-stable architecture, complemented by reliably stored qubits and local quantum logic. Furthermore, they achieved real-time communication and feed-forward gate operations across the network. As shown in Fig. 6(e), they demonstrated two quantum network protocols that do not require post-selection: one is the creation of a GHZ

state among three nodes, and the other involves entanglement swapping via an intermediate node.[33]

C. Fault-tolerant quantum networks: Overcoming resource limitation

As the network scale increases, the required quantum node resources grow exponentially. In 2008, researchers proposed a fault-tolerant quantum network protocol,[180] which requires only two qubits to form a quantum node, significantly reducing node resource requirements. They also demonstrated how to implement this protocol in diamonds using NV center electron spins and a nuclear spin to form a two-qubit node. Furthermore, Rozpedek *et al.* proposed three repeater schemes, as shown in Fig. 6(f),[181] and evaluated their key distribution capabilities in recent NV center experiments. The results showed that the single-photon scheme performed the best. Using methods to suppress loss and operational errors, Muralidharan *et al.* categorized quantum repeaters into three generations,[182] comparing their costs under various physical parameters. Among these, solid-state color centers like diamond NV centers are particularly suited for first and second-generation repeaters due to their deterministic local quantum operations and heralded entanglement experiments. Additionally, quantum error correction techniques necessary for the second-generation and the third-generation repeater have been realized by coupling NV center electron spins with three nuclear spins in 2014.[42]

D. Practical quantum networks: Moving beyond laboratory setups

To realize an efficient quantum network, it is essential to abstract physical layer protocols into operations that users can perform without understanding the underlying principles. This requires a link layer, which abstracts entanglement generated at the physical layer into a user-friendly and clearly defined entanglement transfer service. Dahlberg *et al.* proposed a functional allocation scheme for the quantum network protocol stack and constructed the first physical and link layer protocols.[183] Pompili *et al.* demonstrated the protocols at an entanglement-based quantum network's link and physical layers through remote network nodes in experimental settings.[184] As shown in Fig. 6(g), the network and transport layers construct and maintain the quantum bit transmission channel, while the blue application layer executes specific quantum network functions. They provided a detailed quantum network stack, pointing the way for future network development. These advancements have accelerated the transition of quantum network construction from laboratory experiments to practical communication systems, laying the foundation for developing and testing scalable components and application protocols on future quantum network platforms.

E. Prospects of silicon carbide as a quantum network platform

While silicon carbide (SiC) currently lags behind diamond-based systems in achieving long-distance multi-node entanglement, these defects—including V_{Si} center, VV^0 center, and V^{4+}—exhibit critical features that a quantum network needs. Time-bin encoded spin-photon entanglement has been achieved in the V_{Si} center. Vanadium defects emit in the telecom O-band, enabling low-loss fiber transmission—a critical feature for practical network deployment. Their narrow emission linewidths enhance photon indistinguishability, directly boosting entanglement generation rates. The spin coherence times are improving from microseconds to milliseconds and from seconds to minutes. These durations provide sufficient windows for entanglement operations before decoherence occurs. The 4H-SiC-on-insulator platform further amplifies these advantages through high-Q microresonators, which enhance spin-photon coupling efficiency by optimizing light confinement.

While silicon carbide still faces challenges like short spin coherence times and low photon indistinguishability, advancements in isotopic purification and strain engineering which adapted from optimizations of other solid-state defect systems are actively mitigating these issues. With telecom-compatible emission, CMOS integration capacity, and robust quantum memory characteristics, as defect engineering methodologies mature, SiC is positioned to overcome current rate limitations and presents a unique combination of features for scalable networks.

VII. CONCLUSION AND OUTLOOK

This review examines the advancements and potential of silicon carbide (SiC) in quantum networks, focusing on sample preparation, spin and optical properties, spin-photon interfaces, and on-chip photonic technologies. SiC offers excellent spin and optical properties alongside compatibility with CMOS processes, making it an up-and-coming material platform for quantum technologies. However, several challenges persist in achieving fully operational quantum networks. One of the main obstacles facing quantum nodes is the difficulty of fabricating color centers with long coherence times at high spatial resolution in a scalable way. Additionally, the complex lattice environmental requirements and the underlying physics of spin coherence still necessitate further investigation. The absence of a mature polarization encoding scheme for PL 6 divacancy center or an optimized energy level structure poses a significant challenge for the spin-photon interface. Moreover, while the SiCOI platform has shown potential, producing large-area wafers with consistent uniformity continues to be problematic. Despite significant advancements in linewidth reduction and frequency conversion technologies, integrating these with on-chip devices and cavities remains a considerable hurdle.

To address these challenges, future efforts should prioritize heterogeneous integration of SiCOI with complementary photonic materials such as lithium niobate-on-insulator (LNOI) or silicon nitride (SiN).[30,150,185] LNOI integration could enhance nonlinear optical functionalities (e.g., electro-optic modulation, frequency conversion) while leveraging SiC's spin-photon interfaces, whereas SiN's ultra-low optical loss and broadband transparency may enable hybrid circuits for multiplexed quantum state routing.[186] Such material hybridization would extend SiC's operational wavelengths, improve device versatility, and bridge gaps in scalable photonic integration—critical for multi-node quantum networks.

Notably, SiC has already demonstrated successful spin-photon entanglement based on time encoding, and techniques such as heralded entanglement preparation and quantum state transfer have been verified. Moving forward, the next crucial steps involve improving the optical and quantum properties of SiC color centers while enhancing the rate and fidelity of entanglement generation at the interfaces. Achieving mutual entanglement between nodes will be essential for advancing the scalability of quantum networks. These developments will enable the efficient sharing and transfer of quantum states and lay

the groundwork for constructing more complex quantum network architectures. With its unique properties, SiC holds significant potential for the advancement of quantum photonics integration, positioning it as a promising platform for developing robust, scalable quantum networks in the future.

ACKNOWLEDGMENTS

We acknowledge the support from the Innovation Program for Quantum Science and Technology (No. 2024ZD0302100), the National Key R&D Program of China (Grant Nos. 2021YFA1400802 and 2023YFB2806700), the National Natural Science Foundation of China (Grant Nos. 12304568, 11934012, and 12474499), the Guangdong Basic and Applied Basic Research Foundation (Grant No. 2022A1515110382), the Shenzhen Fundamental research project (Grant Nos. JCYJ20241202123903005 and JCYJ20230807094408018), the Guangdong Provincial Quantum Science Strategic Initiative (GDZX2403004, GDZX2303001, GDZX2306002, GDZX2200001, and GDZX2406002), the Young Elite Scientists Sponsorship Program by CAST, and the New Cornerstone Science Foundation through the XPLORER PRIZE.

AUTHOR DECLARATIONS

Conflict of Interest

The authors have no conflicts to disclose.

Author Contributions

Yu Zhou, Junhua Tan, and HaiBo Hu contributed equally to this work.

Yu Zhou: Conceptualization (equal); Funding acquisition (equal); Supervision (equal); Writing – original draft (equal); Writing – review & editing (equal). **Junhua Tan:** Investigation (equal); Writing – original draft (equal). **HaiBo Hu:** Investigation (equal); Writing – original draft (equal). **Sikai Hua:** Writing – original draft (equal). **Chunhui Jiang:** Writing – original draft (equal). **Bo Liang:** Writing – original draft (equal). **Tongyuan Bao:** Writing – original draft (equal). **Xinfang Nie:** Writing – original draft (equal). **Shumin Xiao:** Resources (equal); Writing – original draft (equal). **Dawei Lu:** Writing – original draft (equal); Writing – review & editing (equal). **Junfeng Wang:** Writing – original draft (equal); Writing – review & editing (equal). **Qinghai Song:** Supervision (equal); Writing – review & editing (equal).

DATA AVAILABILITY

The data that support the findings of this study are available from the corresponding authors upon reasonable request.

REFERENCES

[1]H. J. Kimble, "The quantum internet," Nature **453**, 1023–1030 (2008).
[2]S. Wehner, D. Elkouss, and R. Hanson, "Quantum internet: A vision for the road ahead," Science **362**, eaam9288 (2018).
[3]K. Azuma *et al.*, "Quantum repeaters: From quantum networks to the quantum internet," Rev. Mod. Phys. **95**, 045006 (2023).
[4]L.-M. Duan and C. Monroe, "Colloquium: Quantum networks with trapped ions," Rev. Mod. Phys. **82**, 1209–1224 (2010).
[5]S. H. Wei *et al.*, "Towards real-world quantum networks: A review," Laser Photonics Rev. **16**, 2100219 (2022).
[6]B. M. Terhal, "Quantum error correction for quantum memories," Rev. Mod. Phys. **87**, 307–346 (2015).
[7]X. Mi *et al.*, "A coherent spin–photon interface in silicon," Nature **555**, 599–603 (2018).
[8]J. Borregaard, A. S. Sørensen, and P. Lodahl, "Quantum networks with deterministic spin–photon interfaces," Adv. Quantum Technol. **2**, 1800091 (2019).
[9]A. E. Rugar *et al.*, "Quantum photonic interface for tin-vacancy centers in diamond," Phys. Rev. X **11**, 031021 (2021).
[10]Y. Zhong *et al.*, "Deterministic multi-qubit entanglement in a quantum network," Nature **590**, 571–575 (2021).
[11]J. Niu *et al.*, "Low-loss interconnects for modular superconducting quantum processors," Nat. Electron. **6**, 235–241 (2023).
[12]S. Krastanov *et al.*, "Optically heralded entanglement of superconducting systems in quantum networks," Phys. Rev. Lett. **127**, 040503 (2021).
[13]A. Reiserer and G. Rempe, "Cavity-based quantum networks with single atoms and optical photons," Rev. Mod. Phys. **87**, 1379–1418 (2015).
[14]S. Ritter *et al.*, "An elementary quantum network of single atoms in optical cavities," Nature **484**, 195–200 (2012).
[15]P. Drmota *et al.*, "Robust quantum memory in a trapped-ion quantum network node," Phys. Rev. Lett. **130**, 090803 (2023).
[16]I. V. Inlek, C. Crocker, M. Lichtman, K. Sosnova, and C. Monroe, "Multispecies trapped-ion node for quantum networking," Phys. Rev. Lett. **118**, 250502 (2017).
[17]M. Widmann *et al.*, "Coherent control of single spins in silicon carbide at room temperature," Nat. Mater. **14**, 164–168 (2015).
[18]W. F. Koehl, B. B. Buckley, F. J. Heremans, G. Calusine, and D. D. Awschalom, "Room temperature coherent control of defect spin qubits in silicon carbide," Nature **479**, 84–87 (2011).
[19]D. M. Lukin, M. A. Guidry, and J. Vuckovic, "Integrated quantum photonics with silicon carbide: Challenges and prospects," PRX Quantum **1**, 020102 (2020).
[20]S. Castelletto *et al.*, "Silicon carbide photonics bridging quantum technology," ACS Photonics **9**, 1434–1457 (2022).
[21]A. L. Yi *et al.*, "Silicon carbide for integrated photonics," Appl. Phys. Rev. **9**, 031302 (2022).
[22]C. Liu *et al.*, "All-optical nanoscale thermometry with silicon carbide color centers," Photonics Res. **12**, 1696–1702 (2024).
[23]K. C. Miao *et al.*, "Universal coherence protection in a solid-state spin qubit," Science **369**, 1493–1497 (2020).
[24]D. J. Christle *et al.*, "Isolated spin qubits in SiC with a high-fidelity infrared spin-to-photon interface," Phys. Rev. X **7**, 021046 (2017).
[25]R.-Z. Fang *et al.*, "Experimental generation of spin-photon entanglement in silicon carbide," Phys. Rev. Lett. **132**, 160801 (2024).
[26]D. M. Lukin *et al.*, "Two-emitter multimode cavity quantum electrodynamics in thin-film silicon carbide photonics," Phys. Rev. X **13**, 011005 (2023).
[27]D. M. Lukin *et al.*, "4H-silicon-carbide-on-insulator for integrated quantum and nonlinear photonics," Nat. Photonics **14**, 330–334 (2020).
[28]C. Wang *et al.*, "Soliton formation and spectral translation into visible on CMOS-compatible 4H-silicon-carbide-on-insulator platform," Light **11**, 341 (2022).
[29]M. A. Guidry, D. M. Lukin, K. Y. Yang, R. Trivedi, and J. Vučković, "Quantum optics of soliton microcombs," Nat. Photonics **16**, 52–58 (2022).
[30]E. Pelucchi *et al.*, "The potential and global outlook of integrated photonics for quantum technologies," Nat. Rev. Phys. **4**, 194–208 (2021).
[31]H. Bernien *et al.*, "Heralded entanglement between solid-state qubits separated by three metres," Nature **497**, 86–90 (2013).
[32]S. L. N. Hermans *et al.*, "Qubit teleportation between non-neighbouring nodes in a quantum network," Nature **605**, 663–668 (2022).
[33]M. Pompili *et al.*, "Realization of a multinode quantum network of remote solid-state qubits," Science **372**, 259–264 (2021).
[34]M. Iuliano *et al.*, "Qubit teleportation between a memory-compatible photonic time-bin qubit and a solid-state quantum network node," npj Quantum Inf. **10**, 107 (2024).
[35]W. Pfaff *et al.*, "Unconditional quantum teleportation between distant solid-state quantum bits," Science **345**, 532–535 (2014).

[36]S. Pirandola, R. Laurenza, C. Ottaviani, and L. Banchi, "Fundamental limits of repeaterless quantum communications," Nat. Commun. **8**, 15043 (2017).
[37]M. Takeoka, S. Guha, and M. M. Wilde, "Fundamental rate-loss tradeoff for optical quantum key distribution," Nat. Commun. **5**, 5235 (2014).
[38]H. J. Briegel, W. Dür, J. I. Cirac, and P. Zoller, "Quantum repeaters: The role of imperfect local operations in quantum communication," Phys. Rev. Lett. **81**, 5932–5935 (1998).
[39]X.-M. Hu *et al.*, "Long-distance entanglement purification for quantum communication," Phys. Rev. Lett. **126**, 010503 (2021).
[40]N. Kalb *et al.*, "Entanglement distillation between solid-state quantum network nodes," Science **356**, 928–932 (2017).
[41]F. Riera-Sàbat, P. Sekatski, A. Pirker, and W. Dür, "Entanglement-assisted entanglement purification," Phys. Rev. Lett. **127**, 040502 (2021).
[42]G. Waldherr *et al.*, "Quantum error correction in a solid-state hybrid spin register," Nature **506**, 204–207 (2014).
[43]V. Sivak *et al.*, "Real-time quantum error correction beyond break-even," Nature **616**, 50–55 (2023).
[44]S. Pezzagna and J. Meijer, "Quantum computer based on color centers in diamond," Appl. Phys. Rev. **8**, 011308 (2021).
[45]S. Krinner *et al.*, "Realizing repeated quantum error correction in a distance-three surface code," Nature **605**, 669–674 (2022).
[46]A. Bourassa *et al.*, "Entanglement and control of single nuclear spins in isotopically engineered silicon carbide," Nat. Mater. **19**, 1319 (2020).
[47]N. Morioka *et al.*, "Spin-controlled generation of indistinguishable and distinguishable photons from silicon vacancy centres in silicon carbide," Nat. Commun. **11**, 2516 (2020).
[48]L. Robledo *et al.*, "High-fidelity projective read-out of a solid-state spin quantum register," Nature **477**, 574–578 (2011).
[49]M. Pfender *et al.*, "Protecting a diamond quantum memory by charge state control," Nano Lett. **17**, 5931–5937 (2017).
[50]P. Solanki *et al.*, "Generation of entanglement and non-stationary states via competing coherent and incoherent bosonic hopping," arXiv:2501.09790 (2025).
[51]T. M. Graham *et al.*, "Multi-qubit entanglement and algorithms on a neutral-atom quantum computer," Nature **604**, 457–462 (2022).
[52]W. B. Gao, A. Imamoglu, H. Bernien, and R. Hanson, "Coherent manipulation, measurement and entanglement of individual solid-state spins using optical fields," Nat. Photonics **9**, 363–373 (2015).
[53]J. R. Schaibley *et al.*, "Demonstration of quantum entanglement between a single electron spin confined to an InAs quantum dot and a photon," Phys. Rev. Lett. **110**, 167401 (2013).
[54]P. Laccotripes *et al.*, "Spin-photon entanglement with direct photon emission in the telecom C-band," Nat. Commun. **15**, 9740 (2024).
[55]A. Tchebotareva *et al.*, "Entanglement between a diamond spin qubit and a photonic time-bin qubit at telecom wavelength," Phys. Rev. Lett. **123**, 063601 (2019).
[56]J.-P. So, J. Luo, J. Choi, B. McCullian, and G. D. Fuchs, "Purcell enhancement and spin spectroscopy of silicon vacancy centers in silicon carbide using an ultrasmall mode-volume plasmonic cavity," Nano Lett. **24**, 11669–11675 (2024).
[57]D. O. Bracher, X. Zhang, and E. L. Hu, "Selective Purcell enhancement of two closely linked zero-phonon transitions of a silicon carbide color center," Proc. Natl. Acad. Sci. U. S. A. **114**, 4060–4065 (2017).
[58]I. Chatzopoulos, F. Martini, R. Cernansky, and A. Politi, "High-Q/V photonic crystal cavities and QED analysis in 3C-SiC," ACS Photonics **6**, 1826–1831 (2019).
[59]C. M. Knaut *et al.*, "Entanglement of nanophotonic quantum memory nodes in a telecom network," Nature **629**, 573–578 (2024).
[60]F. Schlawin, D. M. Kennes, and M. A. Sentef, "Cavity quantum materials," Appl. Phys. Rev. **9**, 011312 (2022).
[61]Z. Mu *et al.*, "Observation of binary spectral jumps in color centers in diamond," Adv. Opt. Mater. **8**, 2000495 (2020).
[62]B. Kambs and C. Becher, "Limitations on the indistinguishability of photons from remote solid state sources," New J. Phys. **20**, 115003 (2018).
[63]S. Castelletto *et al.*, "Color centers enabled by direct femto-second laser writing in wide bandgap semiconductors," Nanomaterials **11**, 72 (2020).
[64]Y. C. Chen *et al.*, "Laser writing of scalable single color centers in silicon carbide," Nano Lett. **19**, 2377–2383 (2019).
[65]Q. Y. Luo *et al.*, "Fabrication and quantum sensing of spin defects in silicon carbide," Front. Phys. **11**, 1270602 (2023).
[66]C. P. Anderson *et al.*, "Electrical and optical control of single spins integrated in scalable semiconductor devices," Science **366**, 1225–1230 (2019).
[67]D. J. Christle *et al.*, "Isolated electron spins in silicon carbide with millisecond coherence times," Nat. Mater. **14**, 160–163 (2015).
[68]F. Fuchs *et al.*, "Engineering near-infrared single-photon emitters with optically active spins in ultrapure silicon carbide," Nat. Commun. **6**, 7578 (2015).
[69]J. F. Wang *et al.*, "On-demand generation of single silicon vacancy defects in silicon carbide," ACS Photonics **6**, 1736–1743 (2019).
[70]P. Koller, T. Astner, B. Tissot, G. Burkard, and M. Trupke, "Strain-enabled control of the vanadium qudit in silicon carbide," arXiv:2501.05896 (2025).
[71]P. Cilibrizzi *et al.*, "Ultra-narrow inhomogeneous spectral distribution of telecom-wavelength vanadium centres in isotopically-enriched silicon carbide," Nat. Commun. **14**, 8448 (2023).
[72]J. Ahn *et al.*, "Extended spin relaxation times of optically addressed vanadium defects in silicon carbide at telecommunication frequencies," Phys. Rev. Appl. **22**, 044078 (2024).
[73]T. Astner *et al.*, "Vanadium in silicon carbide: Telecom-ready spin centres with long relaxation lifetimes and hyperfine-resolved optical transitions," Quantum Sci. Technol. **9**, 035038 (2024).
[74]J. F. Wang *et al.*, "Coherent control of nitrogen-vacancy center spins in silicon carbide at room temperature," Phys. Rev. Lett. **124**, 223601 (2020).
[75]S. Castelletto *et al.*, "A silicon carbide room-temperature single-photon source," Nat. Mater. **13**, 151–156 (2014).
[76]G. Calusine, A. Politi, and D. D. Awschalom, "Cavity-enhanced measurements of defect spins in silicon carbide," Phys. Rev. Appl. **6**, 014019 (2016).
[77]J. Wang *et al.*, "Bright room temperature single photon source at telecom range in cubic silicon carbide," Nat. Commun. **9**, 4106 (2018).
[78]H. J. von Bardeleben, J. L. Cantin, E. Rauls, and U. Gerstmann, "Identification and magneto-optical properties of the NV center in 4H-SiC," Phys. Rev. B **92**, 064104 (2015).
[79]S. Zargaleh *et al.*, "Evidence for near-infrared photoluminescence of nitrogen vacancy centers in 4H-SiC," Phys. Rev. B **94**, 060102 (2016).
[80]Z. Mu *et al.*, "Coherent manipulation with resonant excitation and single emitter creation of nitrogen vacancy centers in 4H silicon carbide," Nano Lett. **20**, 6142–6147 (2020).
[81]S. Sato *et al.*, "Formation of nitrogen-vacancy centers in 4H-SiC and their near infrared photoluminescence properties," J. Appl. Phys. **126**, 083105 (2019).
[82]J. F. Wang *et al.*, "Scalable fabrication of single silicon vacancy defect arrays in silicon carbide using focused ion beam," ACS Photonics **4**, 1054–1059 (2017).
[83]H. Kraus *et al.*, "Three-dimensional proton beam writing of optically active coherent vacancy spins in silicon carbide," Nano Lett. **17**, 2865–2870 (2017).
[84]Y. Abdedou *et al.*, "Photoluminescence of femtosecond laser-irradiated silicon carbide," arXiv:2404.09906 (2024).
[85]J. F. Wang *et al.*, "Efficient generation of an array of single silicon-vacancy defects in silicon carbide," Phys. Rev. Appl. **7**, 064021 (2017).
[86]G. Wolfowicz *et al.*, "Vanadium spin qubits as telecom quantum emitters in silicon carbide," Sci. Adv. **6**, eaaz1192 (2020).
[87]C. Babin *et al.*, "Fabrication and nanophotonic waveguide integration of silicon carbide colour centres with preserved spin-optical coherence," Nat. Mater. **21**, 67–73 (2022).
[88]M. Wang *et al.*, "Self-aligned patterning technique for fabricating high-performance diamond sensor arrays with nanoscale precision," Sci. Adv. **8**, eabn9573 (2022).
[89]Z. X. He *et al.*, "Maskless generation of single silicon vacancy arrays in silicon carbide by a focused He ion beam," ACS Photonics **10**, 2234–2240 (2023).
[90]Y. Zhou *et al.*, "Direct writing of single germanium vacancy center arrays in diamond," New J. Phys. **20**, 125004 (2018).
[91]Z. X. He *et al.*, "Robust single modified divacancy color centers in 4H-SiC under resonant excitation," Nat. Commun. **15**, 10146 (2024).
[92]A. F. M. Almutairi, J. G. Partridge, C. L. Xu, I. S. Cole, and A. S. Holland, "Direct writing of divacancy centers in silicon carbide by femtosecond laser irradiation and subsequent thermal annealing," Appl. Phys. Lett. **120**, 014003 (2022).
[93]A. M. Day, J. R. Dietz, M. Sutula, M. Yeh, and E. L. Hu, "Laser writing of spin defects in nanophotonic cavities," Nat. Mater. **22**, 696–702 (2023).

[94]Z.-H. Hao *et al.*, "Laser writing and spin control of near infrared emitters in silicon carbide," ACS Photonics **12**(3), 1552–1560 (2025).
[95]D. D. Awschalom, R. Hanson, J. Wrachtrup, and B. B. Zhou, "Quantum technologies with optically interfaced solid-state spins," Nat. Photonics **12**, 516–527 (2018).
[96]Q. Li *et al.*, "Room-temperature coherent manipulation of single-spin qubits in silicon carbide with a high readout contrast," Natl. Sci. Rev. **9**, nwab122 (2022).
[97]A. L. Falk *et al.*, "Polytype control of spin qubits in silicon carbide," Nat. Commun. **4**, 1819 (2013).
[98]H. Hu *et al.*, "Room-temperature waveguide integrated quantum register in a semiconductor photonic platform," Nat. Commun. **15**, 10256 (2024).
[99]L. P. Yang *et al.*, "Electron spin decoherence in silicon carbide nuclear spin bath," Phys. Rev. B **90**, 241203 (2014).
[100]G. Wolfowicz *et al.*, "Optical charge state control of spin defects in 4H-SiC," Nat. Commun. **8**, 1876 (2017).
[101]V. Ivády *et al.*, "Identification of Si-vacancy related room-temperature qubits in 4H silicon carbide," Phys. Rev. B **96**, 161114 (2017).
[102]M. Widmann *et al.*, "Electrical charge state manipulation of single silicon vacancies in a silicon carbide quantum optoelectronic device," Nano Lett. **19**, 7173–7180 (2019).
[103]M. Atatüre, D. Englund, N. Vamivakas, S.-Y. Lee, and J. Wrachtrup, "Material platforms for spin-based photonic quantum technologies," Nat. Rev. Mater. **3**, 38–51 (2018).
[104]S. Kanai *et al.*, "Generalized scaling of spin qubit coherence in over 12,000 host materials," Proc. Natl. Acad. Sci. U. S. A. **119**, e2121808119 (2022).
[105]S. G. Carter, Ö. Soykal, P. Dev, S. E. Economou, and E. R. Glaser, "Spin coherence and echo modulation of the silicon vacancy in 4H-SiC at room temperature," Phys. Rev. B **92**, 161202 (2015).
[106]D. Simin *et al.*, "Locking of electron spin coherence above 20 ms in natural silicon carbide," Phys. Rev. B **95**, 161201 (2017).
[107]M. Onizhuk *et al.*, "Probing the coherence of solid-state qubits at avoided crossings," PRX Quantum **2**, 010311 (2021).
[108]H. Seo *et al.*, "Quantum decoherence dynamics of divacancy spins in silicon carbide," Nat. Commun. **7**, 12935 (2016).
[109]C. P. Anderson *et al.*, "Five-second coherence of a single spin with single-shot readout in silicon carbide," Sci. Adv. **8**, eabm5912 (2022).
[110]K. C. Miao *et al.*, "Electrically driven optical interferometry with spins in silicon carbide," Sci. Adv. **5**, eaay0527 (2019).
[111]M. Niethammer *et al.*, "Coherent electrical readout of defect spins in silicon carbide by photo-ionization at ambient conditions," Nat. Commun. **10**, 5569 (2019).
[112]T. Nishikawa *et al.*, "Electrical detection of nuclear spins via silicon vacancies in silicon carbide at room temperature," Appl. Phys. Lett. **121**, 184005 (2022).
[113]Y. Zhou *et al.*, "Rapid and unconditional parametric reset protocol for tunable superconducting qubits," Nat. Commun. **12**, 5924 (2021).
[114]A. L. Falk *et al.*, "Optical polarization of nuclear spins in silicon carbide," Phys. Rev. Lett. **114**, 247603 (2015).
[115]V. Ivády *et al.*, "Theoretical model of dynamic spin polarization of nuclei coupled to paramagnetic point defects in diamond and silicon carbide," Phys. Rev. B **92**, 115206 (2015).
[116]V. Ivády *et al.*, "High-fidelity bidirectional nuclear qubit initialization in SiC," Phys. Rev. Lett. **117**, 220503 (2016).
[117]P. V. Klimov, A. L. Falk, D. J. Christle, V. V. Dobrovitski, and D. D. Awschalom, "Quantum entanglement at ambient conditions in a macroscopic solid-state spin ensemble," Sci. Adv. **1**, e1501015 (2015).
[118]D. R. Candido and M. E. Flatté, "Suppression of the optical linewidth and spin decoherence of a quantum spin center in a p-n diode," PRX Quantum **2**, 040310 (2021).
[119]A. Sipahigil *et al.*, "Quantum interference of single photons from remote nitrogen-vacancy centers in diamond," Phys. Rev. Lett. **108**, 143601 (2012).
[120]L. C. Bassett, F. J. Heremans, C. G. Yale, B. B. Buckley, and D. D. Awschalom, "Electrical tuning of single nitrogen-vacancy center optical transitions enhanced by photoinduced fields," Phys. Rev. Lett. **107**, 266403 (2011).
[121]Y. Guo *et al.*, "Electroluminescence of NV by impact excitation and Stark shift in a MIM diamond structure," Appl. Phys. Lett. **119**, 252102 (2021).
[122]A. M. Day *et al.*, "Electrical manipulation of telecom color centers in silicon," Nat. Commun. **15**, 4722 (2024).
[123]C. F. de las Casas *et al.*, "Stark tuning and electrical charge state control of single divacancies in silicon carbide," Appl. Phys. Lett. **111**, 262403 (2017).
[124]M. Rühl, L. Bergmann, M. Krieger, and H. B. Weber, "Stark tuning of the silicon vacancy in silicon carbide," Nano Lett. **20**, 658–663 (2020).
[125]H. Akbari *et al.*, "Lifetime-limited and tunable quantum light emission in h-BN via electric field modulation," Nano Lett. **22**, 7798–7803 (2022).
[126]T. Steidl *et al.*, "Single V2 defect in 4H silicon carbide Schottky diode at low temperature," arXiv:2410.09021 (2024).
[127]Y. Zhou *et al.*, "Room temperature solid-state quantum emitters in the telecom range," Sci. Adv. **4**, eaar3580 (2018).
[128]M. Hollenbach *et al.*, "Wafer-scale nanofabrication of telecom single-photon emitters in silicon," Nat. Commun. **13**, 7683 (2022).
[129]L. Spindlberger *et al.*, "Optical properties of vanadium in 4H silicon carbide for quantum technology," Phys. Rev. Appl. **12**, 014015 (2019).
[130]K. Li, Y. Zhou, A. Rasmita, I. Aharonovich, and W. Gao, "Nonblinking emitters with nearly lifetime-limited linewidths in CVD nanodiamonds," Phys. Rev. Appl. **6**, 024010 (2016).
[131]A. Sipahigil *et al.*, "Indistinguishable photons from separated silicon-vacancy centers in diamond," Phys. Rev. Lett. **113**, 113602 (2014).
[132]A. Sipahigil *et al.*, "An integrated diamond nanophotonics platform for quantum-optical networks," Science **354**, 847–850 (2016).
[133]C. P. Dietrich, A. Fiore, M. G. Thompson, M. Kamp, and S. Höfling, "GaAs integrated quantum photonics: Towards compact and multi-functional quantum photonic integrated circuits," Laser Photonics Rev. **10**, 870–894 (2016).
[134]H. Sato, M. Abe, I. Shoji, J. Suda, and T. Kondo, "Accurate measurements of second-order nonlinear optical coefficients of 6H and 4H silicon carbide," J. Opt. Soc. Am. B **26**, 1892–1896 (2009).
[135]F. Martini and A. Politi, "Four wave mixing in 3C SiC ring resonators," Appl. Phys. Lett. **112**, 251110 (2018).
[136]X. Qian, P. Jiang, and R. Yang, "Anisotropic thermal conductivity of 4H and 6H silicon carbide measured using time-domain thermoreflectance," Mater. Today Phys. **3**, 70–75 (2017).
[137]S. Karmann, R. Helbig, and R. A. Stein, "Piezoelectric properties and elastic constants of 4H and 6H SiC at temperatures 4–320 K," J. Appl. Phys. **66**, 3922–3924 (1989).
[138]B. S. Song *et al.*, "Ultrahigh-Q photonic crystal nanocavities based on 4H silicon carbide," Optica **6**, 991–995 (2019).
[139]Y. Wang, Q. Lin, and P. X. L. Feng, "Single-crystal 3C-SiC-on-insulator platform for integrated quantum photonics," Opt. Express **29**, 1011–1022 (2021).
[140]M. Naftaly, J. F. Molloy, B. Magnusson, Y. M. Andreev, and G. V. Lanskii, "Silicon carbide—A high-transparency nonlinear material for THz applications," Opt. Express **24**, 2590–2595 (2016).
[141]E. Togan *et al.*, "Quantum entanglement between an optical photon and a solid-state spin qubit," Nature **466**, 730–734 (2010).
[142]W. B. Gao, P. Fallahi, E. Togan, J. Miguel-Sanchez, and A. Imamoglu, "Observation of entanglement between a quantum dot spin and a single photon," Nature **491**, 426–430 (2012).
[143]J. Javadzade, M. Zahedian, F. Kaiser, V. Vorobyov, and J. Wrachtrup, "Efficient nuclear spin - photon entanglement with optical routing," arXiv:2408.01824 (2024).
[144]P.-J. Stas *et al.*, "Robust multi-qubit quantum network node with integrated error detection," Science **378**, 557–560 (2022).
[145]X.-Y. Lai *et al.*, "Single-shot readout of a nuclear spin in silicon carbide," Phys. Rev. Lett. **132**, 180803 (2024).
[146]E. Hesselmeier *et al.*, "High-fidelity optical readout of a nuclear-spin qubit in silicon carbide," Phys. Rev. Lett. **132**, 180804 (2024).
[147]J. P. Lee *et al.*, "A quantum dot as a source of time-bin entangled multi-photon states," Quantum Sci. Technol. **4**, 025011 (2019).
[148]M. H. Appel *et al.*, "Entangling a hole spin with a time-bin photon: A waveguide approach for quantum dot sources of multiphoton entanglement," Phys. Rev. Lett. **128**, 233602 (2022).
[149]N. Coste *et al.*, "High-rate entanglement between a semiconductor spin and indistinguishable photons," Nat. Photonics **17**, 582–587 (2023).
[150]J.-H. Kim, S. Aghaeimeibodi, J. Carolan, D. Englund, and E. Waks, "Hybrid integration methods for on-chip quantum photonics," Optica **7**, 291–308 (2020).
[151]C. Wang *et al.*, "High-Q microresonators on 4H-silicon-carbide-on-insulator platform for nonlinear photonics," Light **10**, 139 (2021).

[152]X. Lu, J. Y. Lee, P. X.-L. Feng, and Q. Lin, "High Q silicon carbide microdisk resonator," Appl. Phys. Lett. **104**, 181103 (2014).
[153]D. O. Bracher and E. L. Hu, "Fabrication of high-Q nanobeam photonic crystals in epitaxially grown 4H-SiC," Nano Lett. **15**, 6202–6207 (2015).
[154]B. S. Song *et al.*, "High-Q-factor nano beam photonic crystal cavities in bulk silicon carbide," Appl. Phys. Lett. **113**, 231106 (2018).
[155]M. Bruel, "Silicon-on-insulator material technology," Electron. Lett. **31**, 1201–1202 (1995).
[156]Y. Zheng *et al.*, "High-quality factor, high-confinement microring resonators in 4H-silicon carbide-on-insulator," Opt. Express **27**, 13053–13060 (2019).
[157]A. L. Yi *et al.*, "Wafer-scale 4H-silicon carbide-on-insulator (4H-SiCOI) platform for nonlinear integrated optical devices," Opt. Mater. **107**, 109990 (2020).
[158]T. R. Fan *et al.*, "High-quality integrated microdisk resonators in the visible-to-near-infrared wavelength range on a 3C-silicon carbide-on-insulator platform," Opt. Lett. **45**, 153–156 (2020).
[159]F. Sardi *et al.*, "Scalable production of solid-immersion lenses for quantum emitters in silicon carbide," Appl. Phys. Lett. **117**, 022105 (2020).
[160]M. Radulaski *et al.*, "Scalable quantum photonics with single color centers in silicon carbide," Nano Lett. **17**, 1782–1786 (2017).
[161]D. J. McCloskey *et al.*, "Enhanced widefield quantum sensing with nitrogen-vacancy ensembles using diamond nanopillar arrays," ACS Appl. Mater. Interfaces **12**, 13421–13427 (2020).
[162]A. L. Crook *et al.*, "Purcell enhancement of a single silicon carbide color center with coherent spin control," Nano Lett. **20**, 3427–3434 (2020).
[163]M. N. Gadalla, A. S. Greenspon, R. K. Defo, X. Zhang, and E. L. Hu, "Enhanced cavity coupling to silicon vacancies in 4H silicon carbide using laser irradiation and thermal annealing," Proc. Natl. Acad. Sci. U. S. A. **118**, e2021768118 (2021).
[164]T. Bao *et al.*, "Tunable cavity coupling to spin defects in a 4H-silicon-carbide-on-insulator platform," ACS Photonics **12**, 2988–2996 (2025).
[165]L. Z. Li *et al.*, "Efficient photon collection from a nitrogen vacancy center in a circular bullseye grating," Nano Lett. **15**, 1493–1497 (2015).
[166]A. Barbiero *et al.*, "Polarization-selective enhancement of telecom wavelength quantum dot transitions in an elliptical bullseye resonator," Nano Lett. **24**, 2839–2845 (2024).
[167]J. Hessenauer *et al.*, "Cavity enhancement of V2 centers in 4H-SiC with a fiber-based Fabry-Pérot microcavity," arXiv:2501.04583 (2025).
[168]J. Michaels *et al.*, "Bias-pulsed atomic layer etching of 4H-silicon carbide producing subangstrom surface roughness," J. Vac. Sci. Technol. A **41**, 032607 (2023).
[169]X.-M. Hu, Y. Guo, B.-H. Liu, C.-F. Li, and G.-C. Guo, "Progress in quantum teleportation," Nat. Rev. Phys. **5**, 339–353 (2023).
[170]F. Xu, X. Ma, Q. Zhang, H.-K. Lo, and J.-W. Pan, "Secure quantum key distribution with realistic devices," Rev. Mod. Phys. **92**, 025002 (2020).
[171]K. Heshami *et al.*, "Quantum memories: Emerging applications and recent advances," J. Mod. Opt. **63**, 2005–2028 (2016).
[172]Y. Lei *et al.*, "Quantum optical memory for entanglement distribution," Optica **10**, 1511 (2023).
[173]S. Pirandola, "End-to-end capacities of a quantum communication network," Commun. Phys. **2**, 51 (2019).
[174]H. Bernien *et al.*, "Two-photon quantum interference from separate nitrogen vacancy centers in diamond," Phys. Rev. Lett. **108**, 043604 (2012).
[175]S. D. Barrett and P. Kok, "Efficient high-fidelity quantum computation using matter qubits and linear optics," Phys. Rev. A **71**, 060310 (2005).
[176]P. C. Humphreys *et al.*, "Deterministic delivery of remote entanglement on a quantum network," Nature **558**, 268–273 (2018).
[177]A. J. Stolk *et al.*, "Metropolitan-scale heralded entanglement of solid-state qubits," Sci. Adv. **10**, eadp6442 (2024).
[178]D. Deutsch *et al.*, "Quantum privacy amplification and the security of quantum cryptography over noisy channels," Phys. Rev. Lett. **77**, 2818–2821 (1996).
[179]W. Dür, H. J. Briegel, J. I. Cirac, and P. Zoller, "Quantum repeaters based on entanglement purification," Phys. Rev. A **59**, 169–181 (1999).
[180]L. Childress, J. M. Taylor, A. S. Sørensen, and M. D. Lukin, "Fault-tolerant quantum communication based on solid-state photon emitters," Phys. Rev. Lett. **96**, 070504 (2006).
[181]F. Rozpędek *et al.*, "Near-term quantum-repeater experiments with nitrogen-vacancy centers: Overcoming the limitations of direct transmission," Phys. Rev. A **99**, 052330 (2019).
[182]S. Muralidharan *et al.*, "Optimal architectures for long distance quantum communication," Sci. Rep. **6**, 20463 (2016).
[183]A. Dahlberg *et al.*, in *Proceedings of the ACM Special Interest Group on Data Communication* (Association for Computing Machinery, Beijing, China, 2019), pp. 159–173.
[184]M. Pompili *et al.*, "Experimental demonstration of entanglement delivery using a quantum network stack," npj Quantum Inf. **8**, 121 (2022).
[185]Z. Yu *et al.*, "Silicon nitride assisted tri-layer edge coupler on lithium niobate-on-insulator platform," Opt. Lett. **48**, 3367–3370 (2023).
[186]J. F. Bauters *et al.*, "Ultra-low-loss high-aspect-ratio Si_3N_4 waveguides," Opt. Express **19**, 3163–3174 (2011).